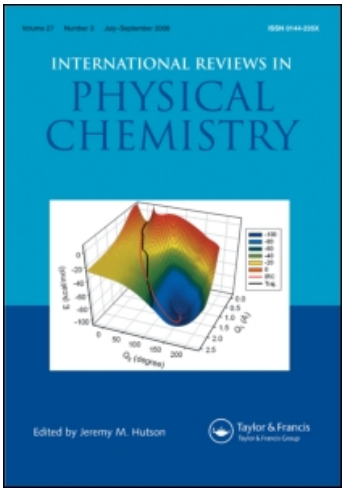

International Reviews in Physical Chemistry
Publication details, including instructions for authors and subscription information:
http://www.informaworld.com/smpp/title~content=t713724383

Vibronic transitions in rare earth spectroscopy

G. Blasse[a]
[a] Debye Research Institute, Utrecht University, Utrecht, The Netherlands

To cite this Article Blasse, G.(1992) 'Vibronic transitions in rare earth spectroscopy', International Reviews in Physical Chemistry, 11: 1, 71 — 100
To link to this Article: DOI: 10.1080/01442359209353266
URL: http://dx.doi.org/10.1080/01442359209353266

INTERNATIONAL REVIEWS IN PHYSICAL CHEMISTRY, 1992, VOL. 11, NO. 1, 71–100

Vibronic transitions in rare earth spectroscopy

by G. BLASSE
Debye Research Institute, Utrecht University,
P.O. Box 80.000, 3508 TA Utrecht, The Netherlands

An overview of the studies of vibronic transitions in the rare earth ions is given with special attention to the intraconfigurational transitions. First the general theory is shortly reviewed, later that of the rare-earth vibronic transitions. The vibronic spectroscopy of Gd^{3+} is extensively dealt with, because it is an ideal ion for this type of study due to its non-degenerate ground state. Vibronic coupling with several vibrational modes has been observed, also with modes in which the central ion is not directly involved. Attention has also been given to Eu^{3+} and Pr^{3+} and some other specific cases of interest. The use of Gd^{3+} as a probe ion is pointed out. A comparison with relating physical phenomena is made. The experimental results are compared with the theoretical expressions derived up till now. The agreement is satisfactory, although of a qualitative nature. The concentration dependence of the vibronic intensity is not well understood. The role of opposite-parity configurations is probably of more importance than generally accepted and the admixture into the $4f^n$ configuration not equal for all its levels.

1. Introduction

Vibronic transitions involve a simultaneous change in the electronic and the vibrational states of the system. In this chapter the system is usually an optically active ion in a host lattice (crystalline or glass) or a solution. The nature of the system is nearly always inorganic. However, most of our considerations are of a more general nature.

The study of vibronic transitions by optical spectroscopy will reveal the interaction between the relevant ion and its surroundings. Unfortunately the literature contains many terms to indicate this interaction, as is often the case in spectroscopy. Here we mention electron–lattice interaction, electron–phonon interaction, vibrational–electronic (or vibronic) interaction, ion-vibration interaction. It is this interaction which is responsible for the difference between free-atom (or free-ion) spectra (sharp lines) and spectra of molecules, ions in solids, etc. (structured bands or broad bands without any structure at all).

If the vibrational–electronic interaction is weak, the spectra will be dominated by sharp lines, especially so at low temperatures. If this interaction is strong, structureless bands are observed which do not reveal much information about the system under study. Famous examples of the latter are the F centre in alkali halides and the tungstate group in $CaWO_4$.

The rare earth ions with optical transitions between levels belonging to the $4f^n$ configuration belong to the weak interaction case. Actually the interaction is usually assumed to be vanishing, and the spectra consist of sharp lines which are purely electronic, i.e. there is no simultaneous change of the vibrational state.

The transition metal ions show an interaction which is usually intermediate between these two extremes. The theory of vibronic transitions in inorganic systems has been developed for an important part on the basis of transition metal ions. A recent book by Henderson and Imbusch (1989) gives a good idea of the present state of the art.

0144-235X/92 $3·00

The question may then arise why somebody should still become interested in the spectroscopy of the weak vibronic transitions of rare earth ions.

The answer to this question may differ from individual to individual, but out of the many reasons to perform such investigations we mention here the following:

(*a*) the 4f electrons are well shielded from the surroundings by the outer $5s^25p^6$ electrons, and it is interesting, therefore, to see what interaction with the (vibrating) surroundings is left at all.

(*b*) the theory of the optical spectra of rare earth ions shows that it is impossible to explain the observations without a certain interaction with the surroundings (parity mixing *via* crystal-field terms, nephelauxetic effect, crystal-field splittings). In itself this is a complicated topic for which we refer to the literature (Peacock 1975, Reisfeld and Jørgensen 1977, Blasse 1987a, Henderson and Imbusch 1989).

(*c*) since there seems to be a weak, but for spectroscopy important, interaction between 4f electrons and the vibrating surroundings, it is of interest to investigate how this interaction depends on the chemical nature of that surroundings.

(*d*) the spectroscopy of rare earth ions finds at the moment a widespread application, and results in a considerable improvement of the quality of luminescent lighting (energy-saving lamps), colour television, X-ray photography, and others (Blasse 1987b, 1989). Since these applications rest on the interaction between the 4f electrons and the surroundings, it is justified to investigate the vibronic transitions of the rare earths ions.

At the end of this review our personal conclusion will be that a study of vibronic transitions in the spectra of rare earths ions is worth while, that it yields interesting information on the behaviour of 4f electrons, and that there is still a lot of work waiting.

This review will be organized as follows. In section 2 we will give a general outline of the theory of vibronic transitions in as simple and general way as possible. This will be illustrated for those who are not acquainted with the field by some experimental results on Cr^{3+}. At the end the expectations for rare earth ions will be given. Section 3 will be devoted to vibronic transitions in rare earth (RE) ions. It will be subdivided as follows: earlier examples of RE vibronic spectra, an outline of the theory, results for Gd^{3+} and a comparison with theory, the use of Gd^{3+} vibronic spectroscopy as a probe of the surroundings, a comparison between the vibronic spectra of isoelectronic Gd^{3+} and Eu^{2+}, vibronic spectra of Eu^{3+}, and the relation between RE vibronic spectroscopy and other physical phenomena. The review will close with a conclusion and outlook.

2. General outline of the theory of vibronic transitions

Optical transitions which involve simultaneously the following two events, viz. a change in the electronic state of the system under study and a change in the vibrational state of that system, are called vibrational–electronic transitions or vibronic transitions. In this review we will use this broad definition. Others use sometimes slightly different definitions introducing terms like sideband, phonon assistance, and replicas. The theory of vibronic transitions is well developed and has been described in many textbooks. As examples we mention here DiBartolo (1968), Lever (1984), Henderson and Imbusch (1989) and the summer school report edited by Flint (1989). Here we have restricted ourselves to inorganic systems.

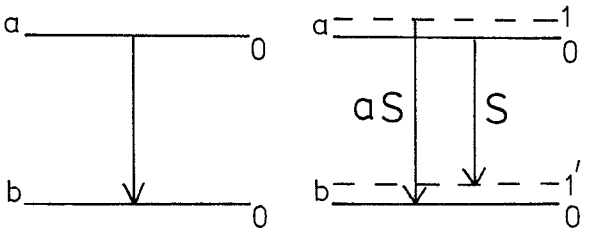

Figure 1. Schematic representation of a zero-phonon transition (left hand side) and the Stokes (S) and anti-Stokes (aS) transitions (right hand side) in emission. The lettering (a, b) denote the electronic states, the numbering $(0, 1, 1')$ the vibrational states.

Let us now consider a vibronic transition (absorption or emission) between the states $\psi(b, n')$ and $\psi(a, n)$ where the final vibrational state n' differs from the initial vibrational state n, and b and a are the final and initial electronic states, respectively. The matrix element for this transition is given by

$$\langle\psi(b, n')|\mu|\psi(a, n)\rangle, \tag{1}$$

where μ is the operator involved (electric-dipole or magnetic-dipole operator).

The optical transition from $a \rightarrow b$ consists, therefore, of a number of vibronic transitions which can be characterized by the vibrational states involved: n–n'. At low temperatures this simplifies to 0–n', since only the $n=0$ vibrational level of the initial electronic state a will be occupied.

The transition to $n'=0$, i.e. 0–0, is called the zero-phonon transition (or 0–0 transition). This one is purely electronic, since no vibrational change is involved. In the spectra they usually occur as very sharp lines. The vibronic transitions 0–n' appear at higher energy (absorption transition) or at lower energy (emission transition). This is shown schematically in figure 1.

At higher temperatures also vibrational levels with $n>0$ occupied in the initial electronic state a. As a consequence the vibronic intensities are temperature dependent. This dependence is given by $(1+\langle n\rangle)$, where $\langle n\rangle$ is the average value of n or the Bose–Einstein factor given by

$$\langle n\rangle = \frac{1}{\exp(h\nu/kT)-1}. \tag{2}$$

Here ν is the frequency of the vibrational mode involved.

The 0–n' transitions occur in emission at lower energy than the 0–0 transition and are, therefore, called Stokes transitions. There is also an anti-Stokes analogon, but only at higher temperatures, i.e. $n(>0) \rightarrow n'=0$ which occurs in emission at an energy higher than the 0–0 transition (see figure 1). Their temperature dependence is given by $\langle n\rangle$. It will be clear that these considerations become more complicated for the more realistic case in which many more than one vibrational mode needs to be considered.

Equation (1) can be simplified to

$$\langle\psi(b)|\mu|\psi(a)\rangle\langle\chi(n')|\chi(n)\rangle, \tag{3}$$

by using the Condon approximation. Here χ denotes the vibrational (or harmonic oscillator) wavefunctions. Equation 3 has several interesting aspects.

In the first place it contains selection rules. We give one example. If we consider intraconfigurational transitions (like in the transition metal and rare earth ions), the

electronic matrix element in (3) (i.e. the first one) vanishes for electric-dipole radiation (parity selection rule). If $n=0$, $|\chi(n)\rangle$ has the totally symmetric representation. This implies that only if $|\chi(n')\rangle$ has the same representation as the electric-dipole operator, (3) does not vanish. Restricting ourselves to inversion symmetry, parity-forbidden electric-dipole transitions can become allowed by interaction with ungerade vibrational modes. Magnetic-dipole transitions may couple with gerade vibrations, but this is not necessary to obtain intensity.

Equation (3) also determines the shape of the optical $a \rightarrow b$ transition. This shape is, for low temperatures, obtained by taking $n=0$ and summing over n'. The result is of the form

$$\frac{\exp(-S)S^{n'}}{(n')!}. \tag{4}$$

S is the Huang–Rhys or coupling parameter and varies from $S=0$ for vanishing coupling to $S \sim 20$–40 for very strong coupling (broad band spectra). Intermediate coupling has $1 < S < 5$. For $S=0$ (4) yields 1, and the spectrum contains only the zero-phonon line. In the intermediate coupling case the zero-phonon line is observable but followed by a series of vibronic lines with equal spacing $E=h\nu$. This is called a progression in the vibrational mode with frequency ν. The strongest line is one of the vibronic lines. At larger values of S the 0–0 transition is usually not observable. Since

$$\sum_{n'} |\langle \chi(n')|\chi(n)\rangle|^2 = 1,$$

the intensity of the $a \rightarrow b$ transition does not depend on S; only its shape does. The intensity of the 0–0 transition is a fraction $\exp(-S)$ of the total intensity. This also makes clear that the vibronic lines in rare earth ion spectra will be very weak: if $S \rightarrow 0$, $\exp(-S) \rightarrow 1$.

We illustrate these considerations by the emission spectrum of Cr^{3+} in the isostructural compounds $GaBO_3$ and $ScBO_3$ (Dirksen *et al.* 1991). In this structure (calcite) the Cr^{3+} ion occupies a site with inversion symmetry. Figure 2 and 3 give these spectra at 4·2 K. In $GaBO_3$ the Cr^{3+} ion feels a strong crystal field and the emission is due to the $^2E \rightarrow {}^4A_2$ transition which occurs within the t_{2g}^3 subconfiguration. Therefore it consists of a sharp line, i.e. $S < 1$. Figure 2 shows indeed a dominating sharp line which is the 0–0 transition, followed by a number of vibronic lines due to coupling with different vibrational modes. These are, among others, lattice mode, and the three ungerade modes of the CrO_6 octahedron (giving vibronically allowed electric-dipole transitions). Remarkable is the feature at 1250 cm^{-1} lower energy than the 0–0 line. This is due to interaction with the ungerade borate stretching mode. Note that the electronic transition (on the Cr^{3+} ion) occurs at a site different from the vibrational transition (the borate group). Such vibronic transitions are sometimes called cooperative vibronic transition (Stavola *et al.* 1981 *a*).

In $ScBO_3$ the Cr^{3+} ion feels a weaker crystal field due to the larger size of the Sc^{3+} ion. The emission consists now of the $^4T_2 \rightarrow {}^4A_2$ transition which occurs between two subconfigurations ($t_{2g}^2\, e_g \rightarrow t_{2g}^3$). This transition belongs to the intermediate coupling scheme. Figure 3 shows the relevant emission spectrum with a weak 0–0 line. On its lower energy side there is a whole collection of vibronic lines. The vibrations involved are the same as for $GaBO_3:Cr^{3+}$ which should be expected for symmetry reasons. The larger S value for Cr^{3+} in $ScBO_3$ follows from the much smaller contribution to the

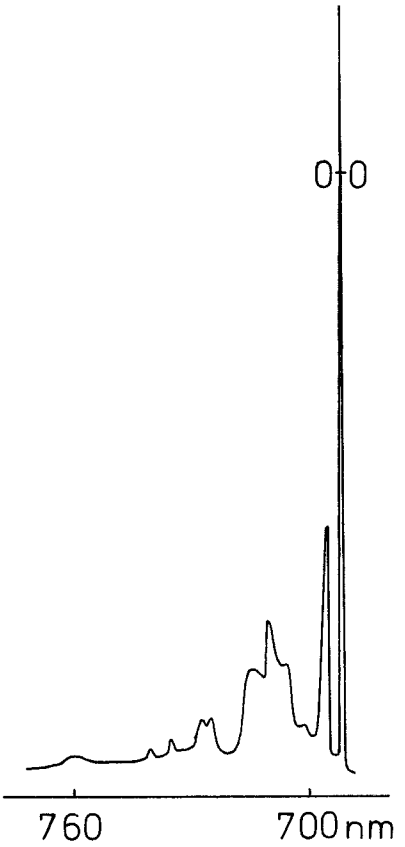

Figure 2. Emission spectrum of $GaBO_3:Cr^{3+}$ at 4·2 K. Note the dominating zero-phonon line. Own measurements.

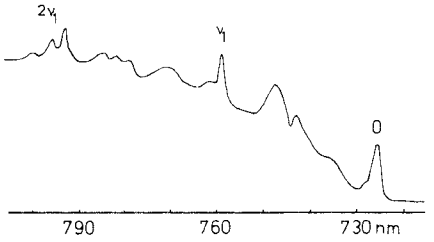

Figure 3. Emission spectrum of $ScBO_3:Cr^{3+}$ at 4·2 K. Note the weak zero-phonon line. Reproduced with permission from Blasse and Dirksen (1988).

total intensity by the 0–0 line. In figure 3 a progression in ν_1 (the totally symmetric CrO_6 vibration) has been indicated. It should be stressed that the 0–0 line, as well as the vibronic lines due to interaction with this ν_1 mode are magnetic-dipole allowed (and electric-dipole forbidden in view of the inversion symmetry at the cation site of calcite).

If vibronic lines are to be observed for the rare earth ions, the spectra are expected to be of the type pictured in figure 2, because also there $S < 1$. Probably the vibronic lines are even much weaker. We are now sufficiently armed to start our considerations on the vibronic transitions in rare earth spectroscopy.

3. Vibronic transitions in rare earth spectroscopy

3.1. *Some earlier experiments*

The literature contains examples of rare-earth vibronic spectra which deserve interest. Here we do not consider the many assignments of vibronic lines in order to explain the presence of too many lines in the spectra, but only those where the interest was focused on the vibronic lines as such.

As early as 1964 Yen *et al.* (1964) reported the vibronic transitions belonging to the $^3H_4 \rightarrow {}^3P_0$ absorption transition of Pr^{3+} in LaF_3 (see figure 4). Note that the total vibronic intensity is of the order of magnitude of the intensity of the electronic zero-phonon line. At that time any further discussion was impossible. In LaF_3 the rare earth ions occupy a crystallographic site without inversion symmetry, so that the relatively strong vibronic intensity is not simply due to a very weak intensity of the zero-phonon line due to the parity selection rule.

The situation is different in the case of Eu^{3+} which has optical transitions with very useful selection rules. For Eu^{3+} on a centre of symmetry the only electronic emission line which can be observed is the magnetic-dipole (MD) transition $^5D_0 - {}^7F_1$. The other lines, and especially $^5D_0 - {}^7F_{0,2}$, turn up with their vibronic transitions only. These selection rules and their consequences for the spectra were studied for some appropriate cases by Blasse *et al.* (1966) and Nieuwpoort *et al.* (1967).

A very detailed study of the vibronic spectroscopy of Eu^{3+} was made by Yamada and Shionoya (1971) for Eu^{3+} in several tungstates. Figure 5 gives the data for Eu^{3+} in

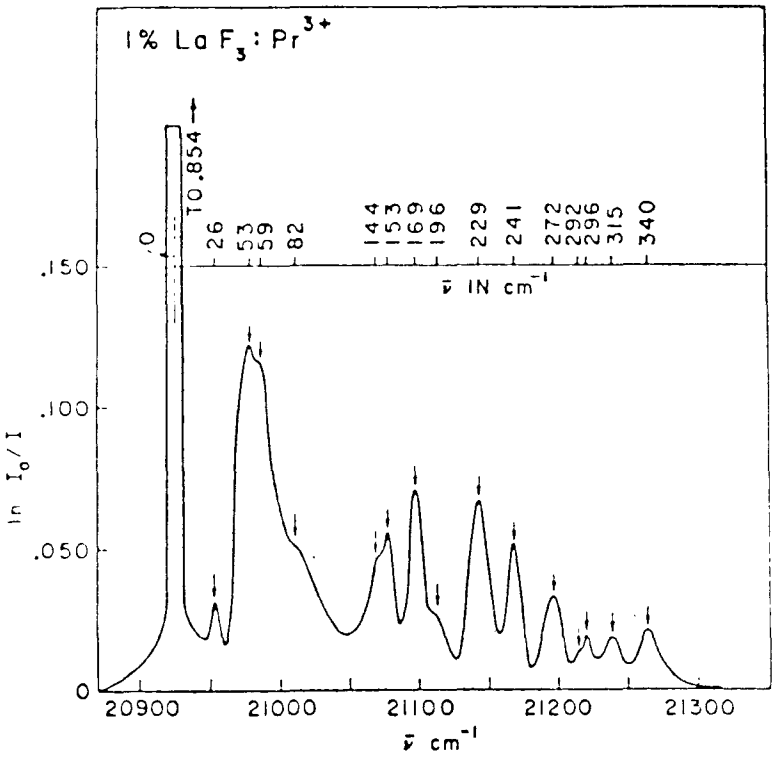

Figure 4. Absorption spectrum of the $^3H_4 \rightarrow {}^3P_0$ transition of Pr^{3+} in LaF_3 at 4·2 K. The zero-phonon transition is on the left-hand side, the others are vibronic transitions. Reproduced with permission from Yen *et al.* (1964).

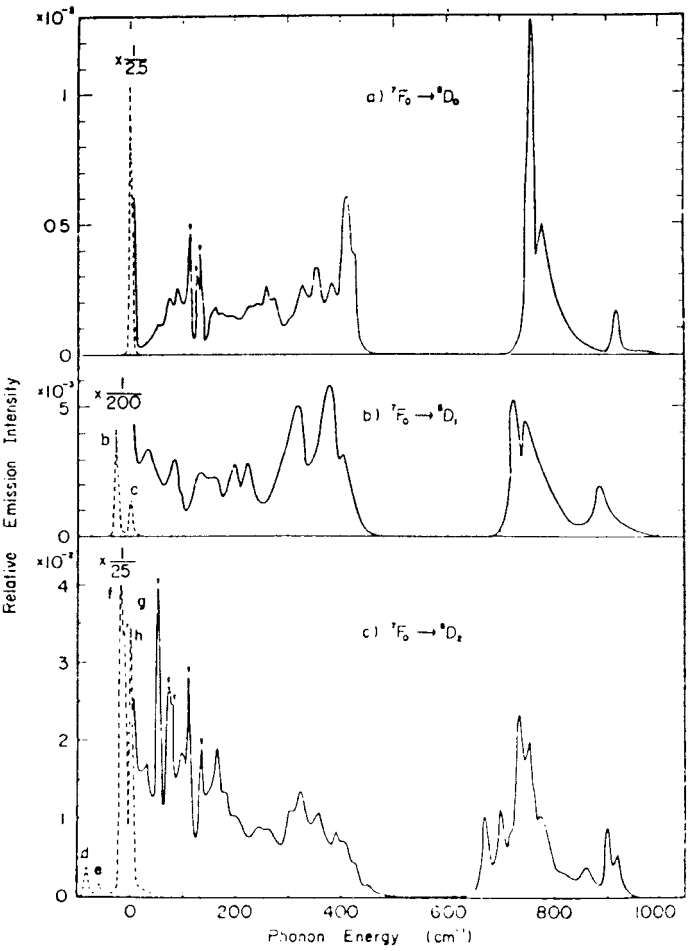

Figure 5. Vibronic lines associated with the electronic transitions $^7F_0 \rightarrow {}^5D_{0,1,2}$ of Eu^{3+} in $CaWO_4$ at 4·2 K. The electronic zero-phonon transitions are indicated by dotted lines. Reproduced with permission from Yamada and Shionoya (1971).

$CaWO_4$ for three transitions. The vibronic lines are numerous but are clearly divided in two groups: one with frequencies below 450 cm^{-1} (lattice vibrations and tungstate bending vibrations), and another with frequencies between 650 and 950 cm^{-1} (tungstate stretching vibrations). The coupling with tungstate vibrations is another example of cooperative vibronic lines.

An impressive study has been performed by Richardson and coworkers in the eighties: they performed experimental and theoretical studies on the electronic and vibronic transitions of all the rare earth ions (except Gd^{3+}) in the host lattice $Cs_2Na(RE)Cl_6$ (see for example Richardson *et al.* (1985), Morley *et al.* (1982), Faulkner and Richardson (1978), Reid and Richardson (1984), and Tanner *et al.* (1991)). This lattice has an undistorted cubic symmetry containing cubic $(RE)Cl_6$ octaedra without Cl^- ions in common. It is an ideal model system to study the optical properties of ions on a site with perfect cubic symmetry. Since pure electronic transitions within the $4f^n$ configuration are completely forbidden, only magnetic-dipole and vibronic transitions are observed. Richardson *et al.* have been able to account for the energy levels, the

Table 1. The $^5D_0$–$^7F_{1,2}$ emission transitions of $Cs_2NaEuCl_6$ at 8·5 K (after data by Morley *et al.* (1982)).

Spectral position (cm^{-1})	Calculated intensity†	Assignment‡	Position relative to 0–0 line (cm^{-1})§
16850	39839	$^5D_0-{}^7F_1$(MD)	0
16600	1	$-\nu_3$	250
16334	f	$^5D_0-{}^7F_2$(E)(ED)	0
16260	6723	$-\nu_4$	74
16232	567	$-\nu_6$	102
16078	8	$-\nu_3$	256
16120	f	$^5D_0-{}^7F_2(T_2)$(ED)	0
16040	844	$-\nu_4$	80
16002	1059	$-\nu_6$	118
15857	6551	$-\nu_3$	263

† relative values; f = forbidden.

‡ MD and ED: magnetic and electric dipole; E and T_2: crystal-field components of $^7F_2$; $-\nu_x$: frequency of the ungerade vibrational mode X of the $EuCl_6^{3-}$ octahedron.

§ zero-phonon line put at $0\,cm^{-1}$.

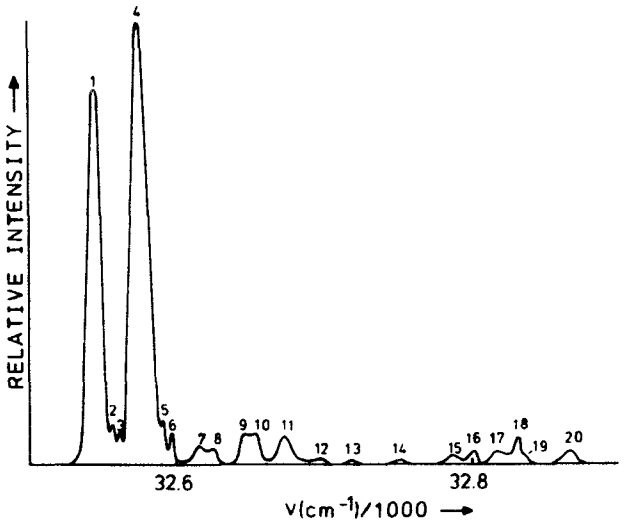

Figure 6. The $^8S_{7/2}\rightarrow{}^6P_{5/2}$ excitation spectrum of the Gd^{3+} emission of $Cs_2NaGdCl_6$ at 4·2 K. The zero-phonon lines are 1 and 4, the others are vibronic. Reproduced with permission from de Vries and Blasse (1988).

crystal-field splittings, the spectral intensities, etc. Table 1 summarizes some of the more important data for Eu^{3+} in $Cs_2NaEuCl_6$. The magnetic-dipole $^5D_0$–$^7F_1$ emission transition is dominating, its vibronic transitions are practically absent; the electric-dipole $^5D_0$–$^7F_2$ emission transitions are absent as pure electronic transitions, but their vibronic transitions are observed. Coupling is to the ungerade vibrations of the octahedral $EuCl_6$ complex.

The spectra of $Cs_2NaGdCl_6$ were reported later by de Vries and Blasse (1988). Figure 6 shows the excitation (= absorption) spectrum of the Gd^{3+} emission for the

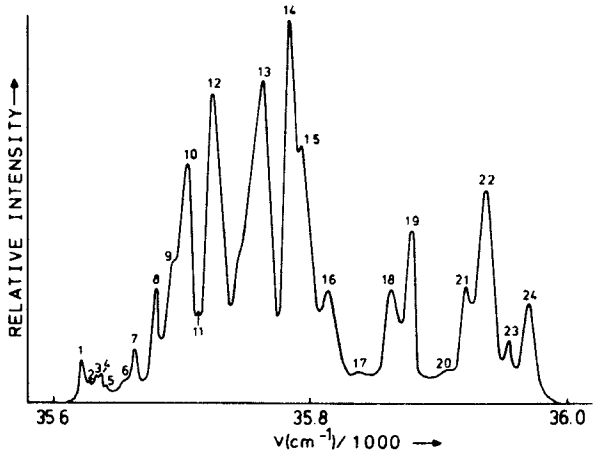

Figure 7. The $^8S_{7/2} \rightarrow {}^6I_{7/2}$ excitation spectrum of the Gd^{3+} emission of $Cs_2NaGdCl_6$ at 4·2 K. The zero-phonon lines are 1, 8 and 11, the others are vibronic. Reproduced with permission from de Vries and Blasse (1988).

transition $^8S_{7/2} \rightarrow {}^6P_{5/2}$ (MD). The electronic lines 1 and 4 dominate. In figure 7 the $^8S_{7/2} \rightarrow {}^6I_{7/2}$ transition is given which is forbidden as a MD transition. Because of the parity selection rule it is also forbidden as an ED transition. The vibronic lines dominate the spectrum.

Interestingly enough the two-photon absorption spectra are completely different (Bouazaoui *et al.* 1991, Kundu *et al.* 1991). In these spectra only the zero-phonon transitions are observed due to a reversal in the parity selection rule in going from one-photon spectroscopy (operator er) to two-photon spectroscopy (operator $(er)^2$).

Hall *et al.* (1982) reported on the vibronic spectra of Gd^{3+} in metaphosphate glasses and compared the results with the Raman spectra of these glasses. It turns out that the vibronic transitions in which vibrational modes are involved that are expected to be infrared active are dominating. Verweij *et al.* (1989) came to a similar conclusion.

Finally we mention work by the group of Caro (Caro *et al.* 1985). This is an impressive compilation of many data, not only on non-molecular solids, but also on coordination compounds. Especially for Nd^{3+} and Pr^{3+} rather intense vibronic transitions were reported.

Let us now, after summarizing these experimental results, have a look at the state of the theory of rare earth vibronic transitions.

3.2. *Theory of vibronic transitions in rare earth ions*

Following Miyakawa (1973) two contributions to the vibronic transition probability can be distinguished. They are shown schematically in figure 8. Usually they are indicated as the M and the Δ process. The former describes a vibronically-induced forced ED transition: coupling of an infrared-active vibrational mode leads to mixing of opposite-parity wavefunctions into those of the $4f^n$ levels. In the latter the occurrence of vibronic transitions is due to a change in the equilibrium position of the excited state relative to the ground state. This Δ process is also known as the Frank–Condon principle.

The literature contains only a few approaches to describe quantitatively the vibronic intensity of rare earth ions. These are due to Faulkner and Richardson (1978),

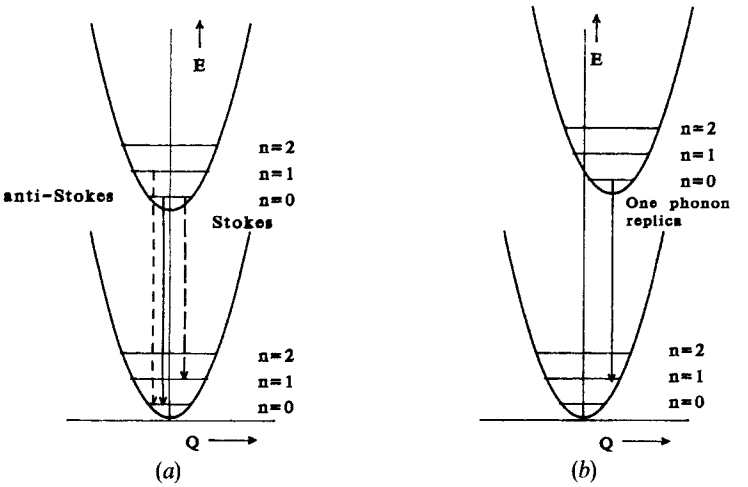

Figure 8. The M process (a) and the Δ process (b). See also text.

Judd (1980), Stavola *et al.* (1981 *a*) and a comparison of the three by Dexpert-Ghys and Auzel (1984).

Faulkner and Richardson gave a general theory of vibronically induced electric-dipole intensity in the f–f transitions of octahedrally (O_h) coordinated trivalent rare earth ions. The model includes static as well as dynamic coupling between the metal ions and the ligands. The calculations relate to elpasolite systems Cs_2NaMCl_6 (M = rare earth ion(s)), which were already mentioned above. The coupling is with the ungerade ν_3, ν_4 and ν_6 vibrational modes of the MCl_6 octahedron. There is good agreement between the experimental results and the calculations.

Judd has put forward a comparable approach for the same system (i.e. a MCl_6 octahedron). In the static coupling he considers the interaction between the 4f electrons on M with a spherical charge distribution with net charge $-ge$ (the ligand) and with the dipoles which are induced in the ligands by the polarising action of the central M^{3+} ion. The induced dipole moment is $3e\alpha\mathbf{r}_j/r_j^3$, where α is the ligand polarisability, and r_j the distance from the M nucleus to the site j of the displaced ligand.

Further he shows that the dynamic-coupling term runs more or less parallel with the static coupling term. The dynamic term becomes more important if the covalency increases. Under certain conditions both terms are of comparable magnitude. We will present the final result below.

Stavola *et al.* added a new element to the discussion by considering cooperative vibronic transitions, i.e. transitions in which there occurs simultaneously an electronic transition within the 4f shell of M and a vibrational transition within the ligand (for which they took OH^- and H_2O). The emission intensity depends on the infrared oscillator strength of the vibration and R^{-6}, where R is the M–ligand distance.

Dexpert-Ghys and Auzel have compared these approaches and have shown that they overlap. The interaction Hamiltonian in the first two approaches is the odd vibrating part of the crystal field, and in the Stavola approach the Coulombic interaction between the M ion and the vibrating molecular species. It is shown that the static part is equivalent in all three approaches. Further these authors state that all approaches neglect the classical one-phonon vibronic replicas (Franck–Condon case),

i.e. only the M process is considered, whereas the Δ process is neglected. Below it will be shown that this point has been well taken.

At the moment we have available a large amount of data on vibronic intensities of certain rare earth ions in many different host lattices. The theoretical approaches are so complicated that they are not very suitable to analyse this type of data satisfactorily. Therefore we have taken the general outcome as a basis for the discussion of this type of data. In the notation of Judd (1980) it runs as follows (Blasse and Brixner 1990 *a*):

$$P_v \sim \nu(g + n\alpha R^{-3})^2 \Xi(1,2)^2 \langle J \| U^{(2)} \| J' \rangle^2 \frac{1}{2J+1} \langle 0 \| T^{(1)} \| p \rangle^2, \tag{5}$$

where P_v is the oscillator strength of the vibronic transition involved, ν its frequency, n the number of ligands around M, g and α the charge and polarisability of the ligand (see above), R the M–ligand distance, $\Xi(1,2)$ is defined by equation (14) in Judd (1962) and takes care of the opposite-parity mixing, J and J' are the total quantum numbers of the initial and final electronic states, the first matrix element is that of the reduced tensor operator $\| U^{(2)} \|$, and the second matrix element that of the electric dipole operator connecting the initial (0) and final (p) vibrational states.

Considering vibronic lines belonging to a certain transition of a given rare earth ion, the J values and the $U^{(2)}$ matrix element will not vary with the ligands. Note, however, that this matrix element imposes a selection rule on the vibronic transitions, $\Delta J = 0, \pm 2$. This implies that vibronic transitions due to the M process obey the selection rule $\Delta J = 0, \pm 2$ which is also the selection rule for hypersensitive (electronic) transitions in rare-earth ions (see, for example, Peacock (1975)). The $T^{(1)}$ matrix element predicts the most intense vibronic lines for coupling with the most infrared-intense vibrational transitions.

The term $(g + n\alpha R^{-3})^2$ is hard to analyse. It will vary less with the nature of the ligands than thought of at first sight. A higher value of g implies a lower value of α; an increase of α will usually mean that R increases too. If we consider one and the same ligand, for example oxygen, the value of α might well be different. This will be discussed below.

Usually the Δ process is neglected for transitions within the $4f^n$ configuration, i.e. the Huang–Rhys parameter is assumed to be 0. There is convincing evidence, from several independent experiments, which shows that this is incorrect. We will come to this point below.

3.3. *Recent experimental work on* Gd^{3+}

In recent years we have performed a study on the vibronic transitions in the emission spectra of the Gd^{3+} ($4f^7$) ion in many host lattices and complexes. The Gd^{3+} ion is extremely suitable for such a study since the ground state $^8S_{7/2}$ is non-degenerate (the splitting of the spin multiplet can be discarded in optical studies). For this reason emission from an excited state, for example from the lowest one, $^6P_{7/2}$, consists at 4·2 K of one electronic line only. Its position is at about 312 nm. All features observed in the spectrum for $\lambda > 312$ nm must be vibronic transitions belonging to the $^6P_{7/2} \rightarrow {}^8S_{7/2}$ transition. This hold of course only if the system to be studied is selected with care so that only one type of Gd^{3+} ions is present.

The experimental conditions for this study are different from those for the other rare earth ions due to the fact that the excited levels of the Gd^{3+} ion are all in the ultraviolet part of the spectrum and the optical transitions involved are all very weak (oscillator strengths in between 10^{-7} and 10^{-8}).

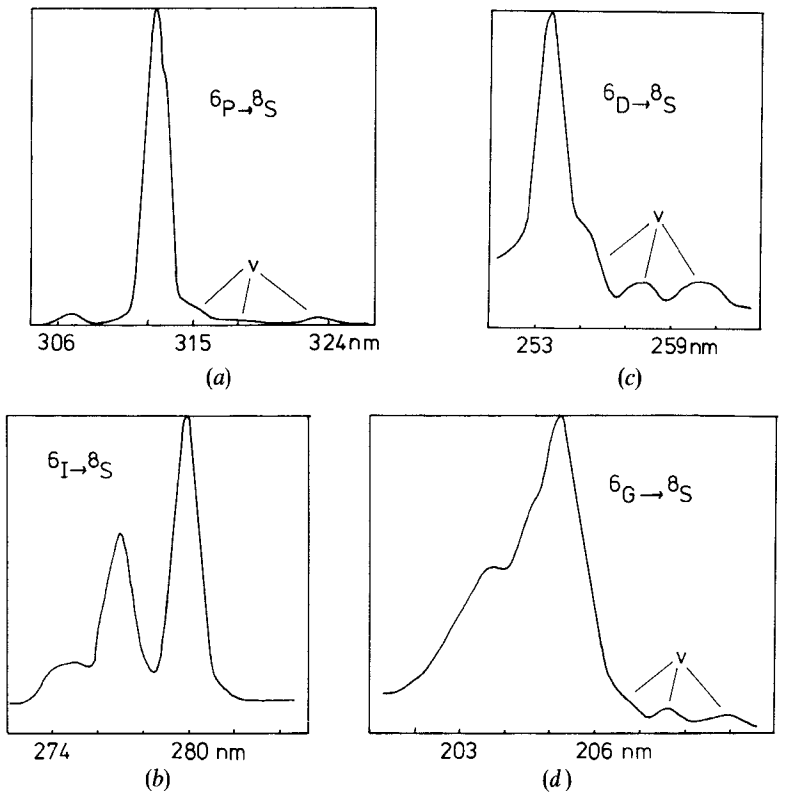

Figure 9. The $^6P \rightarrow {}^8S$, $^6D \rightarrow {}^8S$, $^6I \rightarrow {}^8S$ and $^6G \rightarrow {}^8S$ emission transitions of Gd^{3+} in $GdPO_4$ at 300 K under X-ray excitation. Vibronic transitions are indicated by v. Reproduced with permission from Brixner and Blasse (1989).

Two approaches were used, the use of a tunable ultraviolet laser (a frequency-doubled pulsed dye laser, pumped with a Nd–YAG laser; Sytsma *et al.* (1991)), and X-ray excitation in cooperation with Dr L. H. Brixner of E. I. du Pont de Nemours and Company (Brixner 1987). As a matter of fact the latter one is not selective, but extremely useful results could be obtained.

As a general example we present in figure 9 and table 2 the X-ray excited emission spectrum of $GdPO_4$ at room temperature (Brixner and Blasse 1989). In spite of the rather low resolving power it is clearly observed that the electronic transitions $^6P \rightarrow {}^8S$, $^6D \rightarrow {}^8S$ and $^6G \rightarrow {}^8S$ are accompanied by vibronic transitions. Table 2 shows that the vibrations involved are the PO_4^{3-} stretching and bending modes and a Gd–O mode (which stands for a movement of Gd^{3+} relative to the phosphate groups). The $^6I \rightarrow {}^8S$ transition, however, is not accompanied by vibronic transitions. It is the only transition of the four mentioned for which the matrix element $U^{(2)}$ vanishes (Detrio 1971), i.e. according to equation (5) the intensity of the vibronic transitions vanishes.

Blasse and Brixner (1989 *a*) have presented many other examples of coupling with vibrations in molecular groups like borate, silicate, sulphate, carbonate and water. Results for $GdAl_3B_4O_{12}$ are given in table 3. The vibrational frequencies derived from the vibronic lines are in good agreement with the frequencies observed in the infrared spectrum. The asymmetric borate stretching vibration (ν_3) is split in the infrared spectrum. Only the one with the higher frequency appears in the vibronic spectrum.

Table 2. Assignment of the Gd^{3+} lines in the emission spectrum of $GdPO_4$. After Brixner and Blasse (1989 *b*).

λ (nm)	Transition from tabulated level to ground state	$\tilde{\nu}$ (cm^{-1})
≈186·0†	$J=3/2$	53·760
≈203·5	$^6G_{11/2,9/2,5/2}$	49·140
205·25	$^6G_{7/2}(e^{11})$	48·720
≈206·5	$(e^{11})-300\,cm^{-1}$	48·425
≈207·7	$(e^{11})-575\,cm^{-1}$	48·145
≈209·5	$(e^{11})-1000\,cm^{-1}$	47·730
253·75	$^6D_{9/2}(e^1)$	39·410
≈255·5	$(e^1)-270\,cm^{-1}$	39·140
≈257·5	$(e^1)-580\,cm^{-1}$	38·830
≈260·5	$(e^1)-1000\,cm^{-1}$	38·390
274·5	$^6I_{11/2,13/2,15/2}$	36·430
277·0	$^6I_{9/2,17/2}$	36·100
280·0	$^6I_{7/2}$	35·715
307·0	$^6P_{5/2}$	32·575
312·6	$^6P_{7/2}(e)$	31·990
≈315·5	$(e)-300\,cm^{-1}$ (vGd–O)	31·695
≈318·0	$(e)-540\,cm^{-1}$ ($\nu_b PO_4^{3-}$)	31·450
323·25	$(e)-1050\,cm^{-1}$ ($\nu_s PO_4^{3-}$)	30·935

† This observation relates to YPO_4:Gd, not to $GdPO_4$.

Table 3. The $^6P_{7/2}\rightarrow{}^8S$ emission spectrum of Gd^{3+} in $GdAl_3B_4O_{12}$ (300 K, X-ray excitation). After Blasse and Brixner (1989 *a*).

Position (cm^{-1}) of emission	Assignment	Infrared spectrum (cm^{-1})
31·900 (e)	$^6P_{7/2}\rightarrow{}^8S$	
e−305, e−460	ν(Gd–O)	
e−735	$\nu_2, \nu_4(BO_3^{3-})$	720
e−990	$\nu_1(BO_3^{3-})$	980
e−1365	$\nu_3(BO_3^{3-})$	1250, 1380

This can be explained as follows. The molecular symmetry of the BO_3^{3-} ion (D_{3h}) is lowered in the crystal, so that the degenerate ν_3 mode splits: the 1380 cm^{-1} component is located mainly in the B–O bonds pointing to Gd^{3+}, the 1250 cm^{-1} component in the B–O bond pointing to two Al^{3+} ions. This explains why the electronic transition on Gd^{3+} couples mainly with the 1380 cm^{-1} component. Since the distance dependence of the vibronic intensity is given by R^{-6}, and R is estimated to differ about a factor two for the two components, the different way of coupling is simply explained by the different distances to the Gd^{3+} ions.

Coupling with the vibrations of organic ligands has also been observed (Blasse and Brixner 1990 *b*). In gadolinium acetate tetrahydrate, $Gd(CH_3COO)_3 \cdot 4H_2O$, for example, there are vibronic transitions due to coupling with the $-(COO)^-$ asymmetric stretching mode and with the bending modes. In addition there is a vibronic transition due to coupling with the H_2O stretching mode. The latter is situated far from the 0–0

transition due to the high frequency of the O–H stretching mode (3235 cm^{-1}): 348 and 313 nm, respectively.

The vibronic transition due to coupling with the water vibration was also studied in $Gd_2(SO_4)_3.8H_2O$ (Brixner *et al.* 1990). The emission spectrum shows vibronic transitions due to coupling with Gd–O, sulphate and H_2O vibrational modes. The Gd^{3+} ion is eight coordinated by oxygen, four of these belonging to water molecules, the other four to sulphate ions.

Upon dehydrating this octahydrate, the vibronic transitions in which water vibrations are involved disappear. By hydrating $Gd_2(SO_4)_3$ with D_2O they reappear but at the expected lower frequency (2440 cm^{-1} instead of 3330 cm^{-1}). This proves directly the role of the water molecule in these transitions.

It has even been possible to observe in the Gd^{3+} emission spectrum vibronic lines due to coupling with vibrations in the second coordination sphere, i.e. at rather long distances. The first example is $Gd(ClO_4)_3.6H_2O$ (Blasse and Brixner 1989 *b*). The Gd^{3+} ion is in this crystal structure octahedrally coordinated by six water molecules. The $[Gd(H_2O)_6]^{3+}$ species form a cubic close packing. The ClO_4^- ions fill all the available octahedral and tetrahedral holes in the close packing. The distances of importance are the following: Gd–O(water) 6 × 2·35 Å, Gd–Cl (centre of ClO_4^- ion in tetrahedral hole) 4 × 4·22 Å, Gd–Cl (centre of ClO_4^- ion in octahedral hole) 6 × 5·96 Å.

The X-ray excited emission spectrum of $Gd(ClO_4)_3.6H_2O$ at 300 K is shown in figure 10. Note the presence of vibronic transitions due to H_2O vibrations (first coordination sphere) and ClO_4^- vibrations (second coordination sphere). Their relative intensities can be accounted for on basis of an R^{-6} distance dependence (compare equation (5)). This is one of the few example of a direct influence of the second coordination sphere on the properties of the well-shielded 4f electrons.

The other example is in the chloride $(NH_4)_2GdCl_5$ (Blasse and Dirksen 1992). In this compound there are $GdCl_6^{3-}$ octahedra in which the Gd^{3+} ions are shielded from the further surroundings by the large Cl^- ions. Nevertheless the photo-excited emission spectrum shows not only vibronic transitions due to coupling with the Gd–Cl vibrations, but also due to the NH_4^+ bending and stretching vibrations, i.e. vibrations in the second coordination sphere.

A very special case turns out to be $Y(OH)_3:Gd^{3+}$. The X-ray excited emission spectrum of this composition has been reported by Blasse *et al.* (1989 *a*). It consists of the $^6P_{7/2} \rightarrow {}^6S_{7/2}$ electronic emission line accompanied by a strong vibronic line at

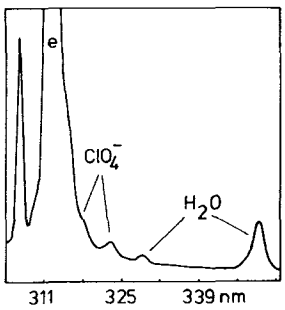

Figure 10. The X-ray excited emission spectrum of $Gd(ClO_4)_3.6H_2O$ at 300 K. The zero-phonon transition is indicated by e. The sharp line on the left is the $^6P_{5/2} \rightarrow {}^8S$ transition, the others are vibronic transitions belonging to e($^6P_{7/2} \rightarrow {}^8S$). Reproduced with permission from Blasse and Brixner (1989 *b*).

Table 4. Assignment of the lines in the emission spectrum of $Y_2O_2S:Gd$ at 300 K (after Blasse *et al.* 1989 *b*).

Spectral position (cm^{-1}) and intensity†	Assignment
32·300 (m)	$^6P_{5/2} \rightarrow {}^8S$
32·205 (vw)	(e)+485
32·070 (w)	(e)+350
31·950 (w)	(e)+230
~31·850 (w, sh)	(e)+130
31·720 (vvs)	$^6P_{7/2} \rightarrow {}^8S$ (e)
31·590 (m)	(e)−130
31·475 (m)	(e)−245
31·360 (m)	(e)−360
31·220 (m)	(e)−500

† s: strong, m: medium, w: weak, v: very, sh: shoulder.

540 cm^{-1} lower energy. The relative intensity of the latter is 8% of the former. The vibronic line can only be due to coupling with the Gd–O vibrational mode. Surprisingly enough there is at first sight no vibronic feature due to coupling with the OH^- group. Under high magnification this vibronic line can just be osberved at 3570 cm^{-1} lower energy than the electronic line and with a relative intensity of only 0·2%.

The system $Y(OH)_3:Gd^{3+}$ is very suitable for the study of Gd^{3+} vibronic lines. Only two or these are observed. The frequencies of the vibrational modes involved differ an order of magnitude, so that they wil not mix. Further the OH^- vibration is not coupled to other OH^- groups due to the absence of hydrogen bonding in this crystal structure. It will be explained below why the intensity of the cooperative vibronic line including the OH^- vibration is so much weaker than that with the H_2O vibration discussed above. Actually the intensity difference is about an order of magnitude.

Stokes and anti-Stokes vibronic emission lines were observed for Gd^{3+} in Y_2O_2S (Blasse *et al.* 1989 *b*). Table 4 gives the X-ray excited emission pattern at room temperature. It should be remembered that anti-Stokes lines can only be observed at higher temperatures due to their temperature dependence given by $\langle n \rangle$. Since $\langle n \rangle = [\exp(h\nu/kT)-1]^{-1}$, and the maximum vibrational frequency in $Y_2O_2S \sim 500\ cm^{-1}$, room temperature should be a suitable temperature to observe the anti-Stokes lines in $Y_2O_2S:Gd^{3+}$.

However, at room temperature the $^6P_{5/2}$ level (~600 cm^{-1} above the $^6P_{7/2}$ level) is thermally occupied and an electronic line due to the $^6P_{5/2} \rightarrow {}^8S_{7/2}$ transition appears in the spectrum. This is another reason to use a host lattice with maximum vibrational frequency of ~500 cm^{-1}, since otherwise the electronic $^6P_{5/2} \rightarrow {}^8S_{7/2}$ transition overlaps with the anti-Stokes vibronic lines belonging to the $^6P_{7/2} \rightarrow {}^8S_{7/2}$ transition. Table 4 shows that the Stokes and anti-Stokes lines are situated symmetrically around the electronic $^6P_{7/2} \rightarrow {}^8S_{7/2}$ line.

The intensity ratio of the Stokes and anti-Stokes lines is given by $\langle n \rangle/(1+\langle n \rangle)$ as follows from our discussion in section 2. The validity of this expression is demonstrated by the data in table 5. It should be realized that the anti-Stokes lines are extremely weak. There are only a few other reports on these in the literature (Auzel *et al.* 1980, Berry *et al.* 1989).

Table 5. Data on the Stokes and anti-Stokes vibronic lines in the emission spectrum of $Y_2O_2S:Gd$ at 300 K.

$\nu_S(\nu_{AS})$† (cm^{-1})	$\langle n\rangle$‡	$\langle n\rangle/(1+\langle n\rangle)$‡	I_{AS}/I_S§	ν(Eu)‖ (cm^{-1})
—	—	—	—	550
500 (485)	0·09	0·08	0·06	500
360 (350)	0·20	0·17	0·19	360
245 (230)	0·42	0·30	0·32	230/260
130 (130)	1·11	0·53	0·43	~150

† ν_S: vibrational frequency derived from Stokes vibronic line.
ν_{AS}: vibrational frequency derived from corresponding anti-Stokes vibronic line.
‡ $\langle n\rangle=[\exp(h\nu_S/kT)-1]^{-1}$; ν_s is taken, because it is more accurate than ν_{AS}.
§ I_{AS}/I_S presents the ratio of the integrated intensities of the anti-Stokes and Stokes vibronic lines due to coupling with a given vibrational mode. The experimental value of I_{AS}/I_S must be compared with the calculated value of $\langle n\rangle/(\langle n\rangle+1)$.
‖ ν(Eu): vibrational frequency derived by Hoshina *et al.* (1977) from the vibronic lines in the emission spectrum of $Y_2O_2S:Eu^{3+}$.

Another interesting observation on the system $Y_2O_2S:Gd^{3+}$ is that the intensity of the vibronic lines depends on the Gd^{3+} concentration. Considering the total amount of vibronic intensity in the $^6P_{7/2}\rightarrow{}^8S_{7/2}$ transition, the surprising result is that it amounts to 8% for $Y_{1.99}Gd_{0.01}O_2S$, but to 25% for Gd_2O_2S. However, this observation is not unique for rare earth ions.

Auzel *et al.* (1980) observed a doubling of the vibronic interaction going from $x=0.01$ to $x=1.0$ in the system $[(C_4H_9)_4N]_3Y_{1-x}Eu_x(NCS)_6$. Hoshina *et al.* (1977) observed a dramatic increase of the vibronic intensity of transitions on the Eu^{3+} ion in the system $Y_{2-x}Eu_xO_2S$.

Van Vliet and Blasse (1990) reported an increase of a factor four of the vibronic intensities in the emission spectrum of Eu^{3+} in the solid solution series $Na_5Gd_{1-x}Eu_x(WO_4)_4$ from $x=0.01$ to $x=1.0$. In the crystal structure of this series the shortest Eu–Eu distance is 6·5 Å and the ions are separated from each other by a tungstate group. This indicates that long-range interactions between the 4f electrons of different rare earths ions must be involved which is rather surprising.

For Pr^{3+} such effects were reported by Donega and Blasse (1991) and Galczynski and Strek (1991). Here the interaction range between the Pr^{3+} ions was estimated to be some 10 Å. We will return to this concentration dependence below.

Above we introduced already the elpasolite lattice of compounds $Cs_2Na(RE)Cl_6$ which is attractive for optical studies because of the cubic site symmetry of the ions of interest (in our case RE^{3+}). This lattice has also an oxygen variant, $Ba_2(RE)TaO_6$ (or the corresponding niobate). For oxides the structure is usually called (1 : 1) ordered perovskite. The Gd^{3+} emission in this lattice has been investigated by Blasse and Brixner (1990 *a*) using X-ray excitation. Table 6 presents an assignment of the emission spectrum of $Ba_2LaTaO_6:Gd^{3+}$. Table 7 shows how the relative intensities of the vibronic lines vary with the choice of the host lattice rare earth ion (La^{3+}, Y^{3+}, Lu^{3+}). Since the ionic radius decreases from La^{3+} to Lu^{3+}, the available size for Gd^{3+} decreases also, i.e. covalency will increase.

In passing we note that Ba_2GdTaO_6 does not show intrinsic Gd^{3+} emission because it is quenched. This is in sharp contrast with isomorphous $Cs_2NaGdCl_6$ (de

Table 6. Assignment of the emission transitions in X-ray excited Ba_2LaTaO_6:Gd at room temperature (Blasse and Brixner 1990*a*).

Position (cm^{-1}) of emission	Assignment	Infrared spectrum (cm^{-1})
36070	$^6I_{11/2} \rightarrow {}^8S$	
35745	$^6I_{9/2,17/2} \rightarrow {}^8S$	
35365	$^6I_{7/2} \rightarrow {}^8S$	
32230	$^6P_{5/2} \rightarrow {}^8S$	
31695	$^6P_{7/2} \rightarrow {}^8S$	
31595	$^6P_{7/2} \rightarrow {}^8S$	
31325	e‡ − 320	$\nu_4(TaO_6)350$
31080	e‡ − 565	$\nu_3(TaO_6)600$
30840	e‡ − 805	$\nu_1(TaO_6)800$
30000†	TaO_6	

† Maximum of broad-band emission.
‡ Average of $^6P_{7/2} \rightarrow {}^8S$ components.

Table 7. Intensity of the vibronic transitions in the emission spectra of the Gd^{3+} ion in Ba_2LnTaO_6 (*Ln* = La, Y, Lu) at 300 K. The ratio *r* gives the integrated vibronic intensity relative to the integrated electronic intensity of the $^6P_{7/2} \rightarrow {}^8S$ transition (Blasse and Brixner 1990*a*).

	La	Y	Lu
$r(\nu_4$ vibronic)	$\sim 0{\cdot}04^5$	$\sim 0{\cdot}05$	$\sim 0{\cdot}06^5$
$r(\nu_3$ vibronic)	$0{\cdot}03^5$	$0{\cdot}05$	$0{\cdot}06^5$
$r(\nu_1$ vibronic)	$0{\cdot}01$	$0{\cdot}01$	$0{\cdot}01$
r(total)	$0{\cdot}09$	$0{\cdot}11$	$0{\cdot}14$

Vries and Blasse 1988) where there is no quenching at all. In the chloride the $GdCl_6$ octahedra are separated from each other by Na^+ ions, in the oxide the GdO_6 octahedra are separated from each other by Ta^{5+} ions. No doubt the Gd–O–Ta–O–Gd configuration allows a stronger interaction between the Gd^{3+} ions than the Gd–Cl–Na–Cl–Gd configuration.

Now we return to tables 6 and 7. The emission spectrum of the Gd^{3+} ion in Ba_2LaTaO_6 shows three vibronic lines due to coupling with the ν_3, ν_4 and ν_1 modes of the tantalate octahedron. The ν_3 and ν_4 modes which are ungerade appear as strong bands in the infrared spectrum, so that their presence in the vibronic spectrum is not unexpected. The symmetric ν_1 mode is not present in the infrared spectrum, i.e. its matrix element $\langle 0 \| T^{(1)} \| p \rangle$ is zero, so that according to (5) the corresponding vibronic line should vanish. Table 7 shows that it is the weakest vibronic line, but also that it is present. Therefore we ascribe that line to the Δ process.

The coupling parameter *S* can now be estimated using (4). Since the relative intensity of the zero-phonon line is e^{-S}, we find $S = 0{\cdot}01$. Such a low value is not unexpected for a rare earth ion.

Table 8. Intensity ratio of the integrated emission intensities of the vibronic transitions and the corresponding zero-phonon transition of Gd^{3+} in oxyhalides for three different electronic transitions. After Blasse *et al.* (1989*c*).

	$^6P_{7/2}\rightarrow{}^8S_{7/2}$	$^6I_{7/2}\rightarrow{}^8S_{7/2}$	$^6D_{9/2}\rightarrow{}^8S_{7/2}$
$LaOCl:Gd^{3+}$	0·16	0·07	0·13
$LaOBr:Gd^{3+}$	0·11	0·03[5]	0·14

Table 9. The ratio r of the total vibronic intensity and the electronic intensity of the $^6P_{7/2}\rightarrow{}^8S_{7/2}$ transition of Gd^{3+} in several host lattices at 300 K.

Composition	r
$Cs_2NaGdCl_6$	0·3
$La_2O_3:Gd^{3+}$	0·25
$LaOCl:Gd^{3+}$	0·16
$Y_2O_3:Gd^{3+}$	0·12
$CaWO_4:Gd^{3+}$	0·09
$BaFBr:Gd^{3+}$	0·08
$GdAl_3B_4O_{12}$	0·08
$ScBO_3:Gd^{3+}$	0·05
$LaAlO_3:Gd^{3+}$	0·02
$[Gd\subset 2.2.1]Cl_3{\cdot}2H_2O$	0·02
$LaF_3:Gd^{3+}$	0·02

Table 7 shows that the increase of the Gd^{3+} covalency influences the v_3 and v_4 vibronic lines, but not the v_1 vibronic line which suggests again that the latter is from different origin.

Further evidence for vibronic lines due to the Δ process originates from a different observation. In the host lattices (RE)OX (X = Cl, Br) the Gd^{3+} ion shows emission from several higher levels, a.o. from the $^6I_{7/2}$ level (Blasse *et al.* 1989). Table 8 gives an overview. Note first that the total vibronic intensity may be as large as some 15% of the corresponding electronic intensity.

The $^6P_{7/2}$, $^6D_{9/2}\rightarrow{}^8S_{7/2}$ transitions are magnetic-dipole transitions, the electric-dipole character of which is determined by the matrix element of the reduced tensor operator $\|U^{(2)}\|$ (compare (5)), whereas the $^6I_{7/2}\rightarrow{}^8S_{7/2}$ transition has only electric-dipole character and an intensity determined by $\|U^{(6)}\|$ (Detrio 1971). This implies that according to (5) the $^6I_{7/2}\rightarrow{}^8S_{7/2}$ transition cannot have vibronic lines due to the M process. The observed lines must be due to the Δ process which will also be responsible for part of the intensity of the vibronic lines belonging to the other transitions.

In this laboratory we have also studied how the vibronic intensity of the Gd^{3+} ion depends on the nature of the ligands. This intensity varies about two orders of magnitude which is a surprising result for the well-shielded 4f electrons. The results have been given in two ways. First the intensity ratio r of the vibronic transitions to the electronic transition has been given (Blasse and Brixner 1990*a*). Table 9 gives some examples. A few cases have been studied in more detail and absolute transition probabilities have been derived for the vibronic transitions (Sytsma *et al.* 1991).

By measuring the decay time as well as the emission spectrum, these transition probabilities can be derived immediately, because the Gd^{3+} ion has another attractive

Table 10. Data on the Gd^{3+} $^6P_{7/2}$ emission in several compositions: investigated compositions, integrated intensity ratios of the vibronic part of the spectrum and the zero-phonon line, and radiative transition probabilities separated into A_{zp}^{ED} and A_{vibr} at 4·2 K (after Sytsma *et al.* (1991)).

Sample	$\frac{Int(vib)}{Int(z.p.)}$ r	Forced ED contributions in A_r† $A_{zp}^{ED}(s^{-1})$	Vibronic rate $A_{vibr}(s^{-1})$	Position of barycentre of $^6P_{7/2}(cm^{-1})$
$LaF_3:Gd^{3+}$	0·02	—	2	32 188
$LiYF_4:Gd^{3+}$	0·04	—	6	32 118
$LaAlO_3:Gd^{3+}$	0·02	175	7	32 000
$Cs_2NaGdCl_6$	0·3	—	28	31 966
$La_2O_3:Gd^{3+}$	0·15	317	63	31 882
$YOCl:Gd^{3+}$	0·23	494	114	31 933

† The magnetic-dipole contribution to this transition equals $A_{zp}^{MD} = 122\,s^{-1}$ (Detrio 1971).

property: non-radiative transitions from the excited levels to the ground state can be neglected completely because of the large energy gap involved ($\Delta E(^6P_{7/2}-{}^8S_{7/2}) = \sim 32\,000\,cm^{-1}$).

Results are given in table 10. The total radiative rate of the $^6P_{7/2} \rightarrow {}^8S_{7/2}$ transition, A_r, is given by

$$A_r = A_{zp}^{MD} + A_{zp}^{ED} + A_{vibr.} \tag{7}$$

Here $A_{vibr.}$ denotes the vibronic contribution to the total rate, whereas the electronic contribution is given by $A_{zp}^{MD} + A_{zp}^{ED}$, the electronic magnetic-dipole and the electronic electric-dipole contribution, respectively. The value of A_{zp}^{MD} is in good approximation independent of the lattice, and amounts to $122\,s^{-1}$ (Detrio 1971). The value of A_{zp}^{ED} varies from 0 (Gd^{3+} on an inversion symmetry site) *via* low values (fluorides) to about $500\,s^{-1}$. The vibronic rate varies about two orders of magnitude.

The position of the $^6P_{7/2}$ level tells us something about the degree of covalency: the lower the $^6P_{7/2}$ level, the higher the degree of covalency (nephelauxetic effect; Antic-Fidancev *et al.* (1987)). Table 10 shows therefore also that $A_{vibr.}$ increases with the degree of covalency.

Before discussing how far the results obtained are confirmed by existing theories, we note that Sytsma *et al.* (1991) also determined the temperature dependence of the intensity of the vibronic lines under discussion. This appears to agree with theory. Figure 11 shows, as an example, the experimental values for the intensity of the anti-Stokes vibronic line of Gd^{3+} in $LiYF_4$ due to coupling with the $330\,cm^{-1}$ vibrational lattice mode. The solid line gives a fit to $\langle n \rangle$ using the vibrational frequency as fit parameter. This yields $\nu = 324\,cm^{-1}$, an excellent agreement.

3.4. *Comparison with theory*

In this section we try to explain several of the experimental results discussed in the previous section using equation (5) given in section 3.2.

A first issue is the matrix element $\langle 0 \| T^{(1)} \| p \rangle$ in (5) which predicts the strongest vibronic lines for coupling with vibrations which show strong infrared absorption. Actually we presented several examples above, for example, the intense vibronic lines due to coupling with the infrared-active ν_3 and ν_4 octahedral modes of the tantalate group in $Ba_2LaTaO_6:Gd^{3+}$.

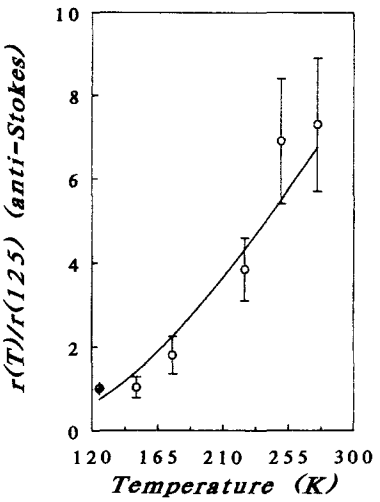

Figure 11. The relative intensity of the anti-Stokes vibronic line at 330 cm^{-1} from the zero-phonon line ($^6P_{7/2} \rightarrow {}^8S$) of Gd^{3+} in $LiYF_4$ as a function of temperature. The solid line is a fit to $\langle n \rangle$. Reproduced with permission from Sytsma *et al.* (1991).

Another nice illustration is the intensity of the vibronic line due to coupling with the OH^- streching vibration. In $Y(OH)_3 : Gd^{3+}$ it is an order of magnitude weaker than in a compound like $Gd_2(SO_4).8H_2O$. However, this is also the case in the infrared spectrum! Equation (5) works very well. The reason for the discrepancy is the absence of hydrogen bonding in $Y(OH)_3$ in contradistinction with $Gd_2(SO_4)_3.8H_2O$. It is well known that hydrogen bonding intensifies the OH streching vibration, and, therefore, the vibronic line under discussion.

This invites us to warn for comparing rare earth vibronic lines with results from Raman spectroscopy which is nowadays often done. From a standpoint of intensity, as given by equation (5), this is in principle incorrect.

Stavola *et al.* (1981 *a*) performed a quantitative calculation of the vibronic intensity due to coupling with OH^-, but compared the results to experiments where H_2O is used as a ligand, which did not result in satisfying results. The Stavola calculation yields for the radiative rate of the vibronic transition due to coupling with one OH^- group 0·08 s^{-1}. This yields for $Y(OH)_3 : Gd^{3+}$ with nine OH^- groups around Gd^{3+} 0·7 s^{-1}. Our experimental results indicate a rate of 0·6 s^{-1}, a very satisfying agreement (Blasse and Brixner 1990 *a*).

The second term in (5) which can be nicely checked is the matrix element of the reduced tensor operator $\|U^{(2)}\|$. The spectrum of $GdPO_4$ is a nice confirmation (table 2 and figure 9). Only the transitions the electric-dipole contribution of which is determined by $\|U^{(2)}\|$ show vibronic lines, and $^6I_{7/2} \rightarrow {}^8S_{7/2}$, determined by $\|U^{(6)}\|$ does not. In $GdPO_4$ the M process is obviously much more important than the Δ process. In other compositions, however, the Δ process contributes considerably (see table 8). We return to this point later.

The other terms appearing in (5) are impossible to vary one by one. Sytsma *et al.* (1991) have shown that a variation of two orders of magnitude of the vibronic intensity by changing the ligands cannot be accounted for by changes in the term $\Xi(1, 2)$ or in the parameters n (number of ligands), R (distance between rare earths ions and ligand) or g (charge of the ligands). The conclusion is that only two mutually connected parameters

can explain this variation, the polarisability α of the ligands and the degree of covalency.

It is important to realize that the value of α depends on the surroundings of the ion. In oxides, for example, the polarisability of the oxide ion increases with the twelfth power of the anion–cation distance in an anisotropic surroundings, and with the third power in an isotropic surroundings. To this we have to add the frequency dependence of α which can be classically presented as

$$\alpha \sim \sum_j \frac{f_{ij}}{v_{ij}^2 - v^2}. \tag{8}$$

Here v is the frequency under consideration, v_{ij} the absorption frequency and f_{ij} the oscillator strength of the electronic transition between the states i and j. This implies that α will increase strongly if the vibronic emission line is situated not too far away from an optical absorption band due to a transition in the immediate surroundings of the rare earth ion.

It is clear that these effects run parallel with covalency. Judd (1980) has shown that vibronic intensity increases with the degree of covalency. This effect is not considered in (5), since it does not contain the dynamic term which becomes important for increasing covalency. Our results present strong evidence that increasing covalency (which may coincide with an increasing value of α) results in higher vibronic intensity. Table 10 shows this most directly as argued above. Also table 7 gives evidence for this effect, since the vibronic transitions due to the *M* process increase in intensity upon shortening the Gd–O distance by using smaller host lattice ions. It is clear that ionic compounds like the fluorides are expected to show weak vibronic lines.

It will be clear that it is a formidable task to account in a quantitative way for the variation of the vibronic intensity with the nature of the ligands.

3.5. *Vibronic spectroscopy of Gd^{3+} as a local probe method*

From experiments described in section 3.3. it has become clear that the Gd^{3+} ion can in principle be used as a probe of its surroundings by virtue of the vibronic part of its emission spectrum. Here we wish to demonstrate the possibilities of this principle on some examples.

Stavola *et al.* (1981 *b*) have studied the Gd^{3+} emission of Gd^{3+} in aqueous solution. It is important again to realize that, in spite of the high streching vibrational frequency of water, non-radiative transitions in Gd^{3+} do not play a role, in contrast with all the other rare earth ions. From the vibronic lines in the emission spectrum Stavola *et al.* were able to derive the stretching frequency of the water molecules which coordinate the Gd^{3+} ion (3315 cm^{-1}). This frequency is different from the other water molecules (3400 cm^{-1}). The difference indicates that the average strength of the hydrogen bonds between water molecules in the first and second hydration spheres of Gd^{3+} is stronger than that of the bulk water.

This method has also been used by Hazenkamp *et al.* (1992) to determine the number of different Gd^{3+} ions in zeolite A and to characterize their surroundings. This is an important applied problem. However, even site-selective excitation techniques are not fully able to solve this problem completely.

Easier to determine is the coordination of Gd^{3+} on a silica surface. The vibronic part of the emission spectrum consists of lines due to coupling with water molecules and lines due to coupling with silicate vibrations (Hazenkamp and Blasse 1990). This

spectrum is given in figure 12. Its interpretation, together with information from the emission of Eu^{3+} in the same situation, is that the rare earth ion is directly bounded to the silica *via* Si–O–Gd bonds and surrounded on the other side by four water molecules.

Another example concerns the cryptates (Blasse *et al.* 1989 *d*). In $[Gd \subset 2.2.1]^{3+}$ in aqueous solution and in the solid state the Gd^{3+} ion is surrounded by the organic 2.2.1 cage. This cage shows three windows through which it has been assumed that water molecules (one per window) coordinate the Gd^{3+} ion. The vibronic part of the emission spectrum consists of lines due to coupling with vibrations of the 2.2.1 cage, but also of lines due to coupling with water vibrations. This is shown in table 11. The low water frequencies indicate strong hydrogen bonding. This is the first direct proof that the water molecules coordinate the Gd^{3+} ion through the cage windows. In passing it is interesting to note that X-ray excitation appeared to be a very efficient excitation source of the solid cryptates.

From these examples it should be clear that vibronic spectroscopy of the Gd^{3+} ion can be a powerful approach in specific cases.

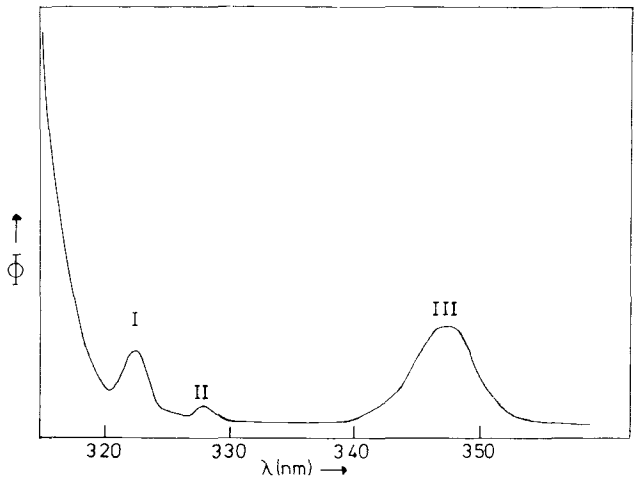

Figure 12. Vibronic lines in the emission spectrum of the $^6P_{7/2} \rightarrow {}^8S_{7/2}$ transition of Gd^{3+} on silica. Line I is due to coupling with Si–O vibrations, lines II and III due to coupling with H_2O vibrations. Reproduced with permission from Hazenkamp and Blasse (1990).

Table 11. Analysis of the X-ray excited emission spectrum of Gd^{3+} in $[Gd \subset 2.2.1]Cl_3 \cdot 2H_2O$ at 300 K.

Spectral position (cm^{-1})	Assignment†
31 975	$^6P_{7/2}$–$^8S_{7/2}$ (electronic)
31 175	e − 800 (cryptand)
30 935	e − 1040 (cryptand)
30 605	e − 1370 (H_2O bending)
29 030	e − 2945 (H_2O stretching)

† e indicates the electronic zero-phonon line.

3.6. *Comparison between $Gd^{3+}(4f^7)$ and $Eu^{2+}(4f^7)$*

A comparison of the spectra of the isoelectronic ions Eu^{2+} and Gd^{3+} has several interesting aspects which are due to the fact that in the case of the divalent ion the opposite-parity configuration $4f^65d$ is close to or even overlaps the lowest emitting level of the $4f^6$ configuration ($^6P_{7/2}$), whereas in case of the trivalent ion it is at high energy: the energy difference between the lowest $4f^65d$ component and the $^6P_{7/2}$ ($4f^7$) level is never more than a few hundred wavenumbers for Eu^{2+}, and at least $30\,000\,cm^{-1}$ for Gd^{3+}.

Recently we made a comparison in this laboratory between the $^6P_{7/2}\rightarrow{}^8S_{7/2}$ emission transition of Gd^{3+} in YOCl and Eu^{2+} in SrFCl and BaFCl (Sytsma and Blasse 1992). The host lattices are isoelectronic which makes a comparison intriguing. The site symmetry involved is C_{4v}, i.e. inversion symmetry is absent. Table 12 presents some relevant results obtained from high-resolution spectroscopy and decay measurements.

Note that the relative vibronic intensity is about equal for the three compositions. However, the radiative electronic rate and the radiative vibronic rate are nearly an order of magnitude larger for the Eu^{2+} ion than for the Gd^{3+} ion. This can be directly related to the lower position of the opposite-parity states of Eu^{2+}, since the intensity has to be stolen from these states (apart from the magnetic-dipole contribution which is relatively small, $\sim 120\,s^{-1}$).

An analysis of the ratio r has been made starting from (5). This shows that in the first approximation r will not depend on the position of the opposite -parity configuration, in agreement with the experimental results (table 12).

In other host lattices the lowest level of the $4f^65d$ configuration of Eu^{2+} is below the $^6P_{7/2}(4f^7)$ level. This has drastic consequences for the emission spectrum. The emission transition is now electric-dipole allowed, the coupling strength increases to the intermediate case. Sometimes vibrational structure cannot be observed, not even at 4·2 K, but sometimes it can. Altogether complicated spectra may result.

As an example we present in figure 13 the emission spectrum of the Eu^{2+} ion in SrB_4O_7 (Meijerink *et al.* 1989). The value of ΔE (table 12) is only $130\,cm^{-1}$. At 4·2 K $^6P_{7/2}\rightarrow{}^8S_{7/2}$ emission occurs followed by a large number of vibronic lines. Their total intensity is about 30% of the total emission intensity. For the greater part they are due to coupling with borate vibrations.

Table 12. Some data on the $^6P_{7/2}\rightarrow{}^8S_{7/2}$ emission transition of Eu^{2+} in SrFCl and BaFCl and Gd^{3+} in YOCl at 4·2 K. After Sytsma and Blasse 1992.

	SrFCl:Eu^{2+}	BaFCl:Eu^{2+}	YOCl:Gd^{3+}
$\Delta E(cm^{-1})$†	700	590	~35 000
$\tau(\mu s)$‡	240	240	1200
r§	0·20	0·16	0·23
$A_{zp}(s^{-1})$‖	3700	3500	490
$A_{vibr}(s^{-1})$¶	740	560	114

† Energy difference between the lowest level of the $4f^65d$ configuration and the $^6P_{7/2}$ level.
‡ decay time of the $4f^7$ ion emission.
§ relative amount of vibronic intensity.
‖ radiative electronic transition rate.
¶ radiative vibronic transition state.

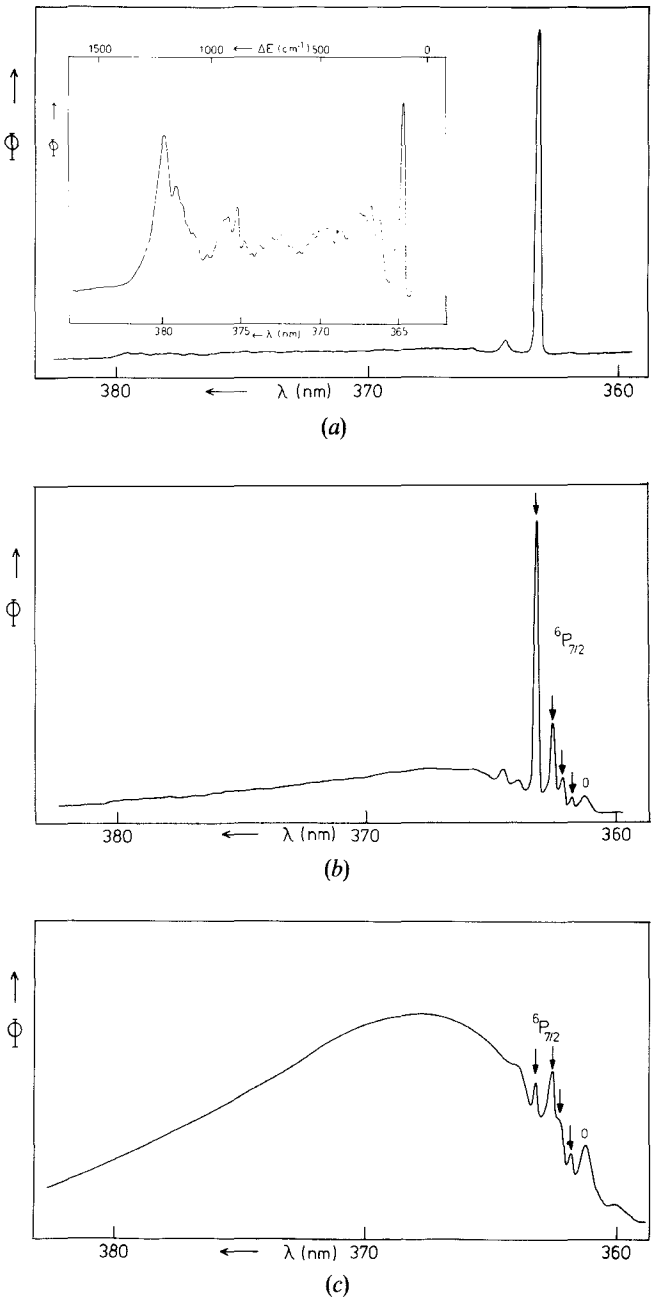

Figure 13. Emission spectra of $SrB_4O_7:Eu^{2+}$ at 4·2 K (*a*), 35 K (*b*) and 110 K (*c*) for 320 nm excitation. The inset is a magnification of the vibronic structure of the $^6P_{7/2} \rightarrow {}^8S_{7/2}$ emission transition. The arrows indicate the crystal-field components of this transition. The zero-phonon line of the broad band is indicated by 0. See also text. Reproduced with permission from Meijerink *et al.* (1989).

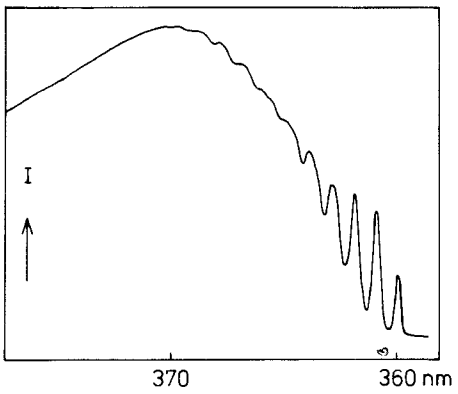

Figure 14. The emission spectrum of $SrB_4O_7:Yb^{2+}$ at 4·2 K. Reproduced with permission from Blasse *et al.* (1990).

At 35 K the emission spectrum contains not one but four zero-phonon-phonon lines indicated by arrows. The low site symmetry of the Sr^{2+} site in SrB_4O_7 is responsible for a fourfold splitting of the $^6P_{7/2}$ level of Eu^{+2}. At 4·2 K only the lowest one is occupied, but at higher temperatures all of them are occupied (the total splitting amounts to some 100 cm^{-1}). Simultaneously a broad band appears with a maximum at 367 nm and a zero-phonon line indicated by 0 (see figure 13). At higher temperatures the band becomes more and more intense compared to the $^6P_{7/2} \rightarrow {}^8S_{7/2}$ lines. The band corresponds to the $4f^6 5d \rightarrow 4f^7$ ($^8S_{7/2}$) emission. The Huang–Rhys coupling parameter S amounts to 4, much larger than for the intraconfigurational transitions (see above).

Illustrative examples can also be found for the alkaline-earth sulfates with Eu^{2+} (Ryan *et al.* 1974, Yamashita *et al.* 1985). $CaSO_4:Eu^{2+}$ shows down to 1·8 K 5d→4f emission with a rich vibrational structure corresponding to the Raman spectrum. Since the electronic zero-phonon line is allowed as electric-dipole transition, the vibronic lines are now expected to be strongest for coupling with Raman-active vibrational modes. In $MgSO_4$ and $BaMg(SO_4)_2$, on the other hand, the emission consists of the $^6P_{7/2} \rightarrow {}^8S_{7/2}$ transition accompanied by weak vibronic lines.

Other rare earth ions with 5d→4f emission show sometimes vibrational structure, for example Ce^{3+} and Yb^{2+}. As a beautiful example we show that of Yb^{2+} in SrB_4O_7 in figure 14 (Blasse *et al.* 1990). There is a clear progression in a frequency of 75 cm^{-1}, yielding $S = 6$. Note the completely different vibrational structure of Yb^{2+} in SrB_4O_7 (electric-dipole allowed transition, intermediate coupling) and Eu^{2+} in SrB_4O_7 at 4·2 K (electric-dipole forbidden transition, weak coupling).

Let us now return to the vibronic transitions in intraconfigurational rare earth spectroscopy and consider other ions than Gd^{3+}.

3.7. *Vibronic transitions in the spectra of other ions*

Blasse (1990) has reviewd the vibronic transitions in the spectra of Eu^{3+} using a large number of data accumulated over many years. For an illustration of these data we refer to figure 15 and table 13 where results for $CsEuMo_2O_8$ are presented. The emission spectrum illustrates the drawback of Eu^{3+} relative to Gd^{3+}. Since the ground manifold ^7F of Eu^{3+} is split into seven levels $^7F_{0-6}$, the vibronic lines belonging to a given electronic transition overlap with another electronic transition.

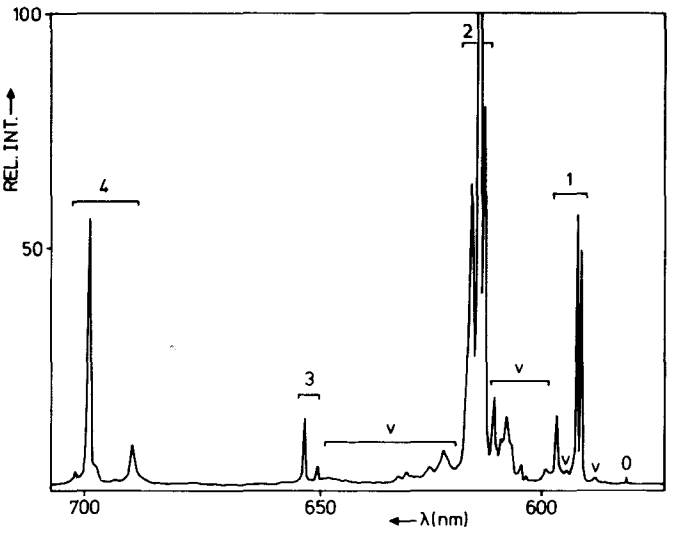

Figure 15. The emission spectrum of $CsEuMo_2O_8$ at 4·2 K. The numbers 0–4 denote the transitions $^5D_0 \rightarrow {}^7F_{0-4}$, whereas v indicates vibronic transitions. Reproduced with permission from van Vliet *et al.* (1988).

Table 13. Vibronic lines in the luminescence spectra of $CsEuMo_2O_8$ at 4·2 K (after van Vliet *et al.* 1988). All values in cm^{-1}.

Excitation spectrum†	Emission spectrum		Assignment vibrational mode
$^7F_0 \rightarrow {}^5D_0$: 17·190	$^5D_0 \rightarrow {}^7F_0$: 17·190	$^5D_0 \rightarrow {}^5F_2$: 16·290	
$^7F_0 \rightarrow {}^5D_0 + 120$			Eu–O
$^7F_0 \rightarrow {}^5D_0 + 150$			Eu–O
$^7F_0 \rightarrow {}^5D_0 + 210$	$^5D_0 \rightarrow {}^7F_0 - 210$	$^5D_0 \rightarrow {}^7F_2 - 210$	Eu–O
$^7F_0 \rightarrow {}^5D_0 + 330$		$^5D_0 \rightarrow {}^7F_2 - 290$	Molybdate bending
$^7F_0 \rightarrow {}^5D_0 + 360$			
$^7F_0 \rightarrow {}^5D_0 + 390$	$^5D_0 \rightarrow {}^7F_0 - 380$		
$^7F_0 \rightarrow {}^5D_0 + 420$		$^5D_0 \rightarrow {}^7F_2 - 410$	
$^7F_0 \rightarrow {}^5D_0 + 680$	$^5D_0 \rightarrow {}^7F_0 - 660$		
$^7F_0 \rightarrow {}^5D_0 + 770$	$^5D_0 \rightarrow {}^7F_0 - 770$	$^5D_0 \rightarrow {}^7F_2 - 760$	Molybdate stretching
$^7F_0 \rightarrow {}^5D_0 + 870$	$^5D_0 \rightarrow {}^7F_0 - 850$	$^5D_0 \rightarrow {}^7F_2 - 850$	
$^7F_0 \rightarrow {}^5D_0 + 930$			

† For the $^7F_0 \rightarrow {}^5D_2$ transition the vibronic spectrum is similar but more complicated due to the splitting of the $^5D_2$ level.

In the case of the Eu^{3+} ion the strongest vibronic lines are observed for the emission transitions $^5D_0 \rightarrow {}^7F_{0,2}$ and the excitation (absorption) transitions $^7F_0 \rightarrow {}^5D_{0,2}$. This agrees with the selection rule for the M process vibronics contained in the $\|U^{(2)}\|$ matrix element (see (5)).

The $^7F_0 \rightarrow {}^5D_1$ absorption and $^5D_0 - {}^7F_1$ emission transitions are magnetic-dipole transitions and forbidden as forced electric-dipole transition (Judd 1962, Ofelt 1962). Therefore, their intensity does not vary much with the surroundings of the Eu^{3+} ion, so that it can be used as a standard for the vibronic intensity. Table 14 gives some results taken from a much more extended table in the original literature (Blasse 1990).

Table 14. Total integrated vibronic intensity in the $^7F_0$–$^5D_2$ and $^5D_0$–$^7F_2$ transitions of the Eu^{3+} ion relative to the corresponding electronic magnetic-dipole transitions for several compositions at 4·2 K. After Blasse (1990).

Composition	$\frac{I(^7F_0–^5D_2)_{vibr}}{I(^7F_0–^5D_1)_e}$	$\frac{I(^5D_0–^7F_2)_{vibr}}{I(^5D_0–^7F_1)_e}$
$SrTiO_3:Eu^{3+}$	$\geqslant 10$	5
$Eu_2Mg_3(NO_3)_{12}\cdot 24H_2O$	> 5	~ 1
$EuNbO_4$	2·8	0·8
$LiEuF_4$	1·7	0·1
$ScBO_3:Eu^{3+}$	1·0	0·65
$GdOCl:Eu^{3+}$	0·9	0·25
$LaAlO_3:Eu^{3+}$	0·4	0·15
$CaSO_4:Eu^{3+}$	$\sim$0·1	0·1

This table shows that also in the case of Eu^{3+} the vibronic intensities vary about two orders of magnitude with the nature of the surroundings. This variation can be understood from (5) (Blasse 1990). The situation is remarkable for $SrTiO_3:Eu^{3+}$ with very strong vibronic transitions. In this host lattice even the $^5D_0$–$^7F_1$ transitions consists for a large part of vibronic transitions which must be due to the Δ process. Table 15 quantifies the results, together with those for some other compositions. From the intensities we can derive a value for the Huang–Rhys coupling parameter S. Although this value is not accurate at all, its magnitude is surprisingly large. Usually a value of $\sim$0·01 is assumed.

The large value of S indicates that the initial and final levels of the transition involved contain different admixtures of other configurations. As a matter of fact this effect will be more pronounced, the lower the energy of the configuration which is mixed in. This is found experimentally (Blasse, 1990, Blasse and Brixner 1990*a*) as can be illustrated here by the last column of table 15. It should be realized that the initial $^5D_0$ level is at about 17 200 cm^{-1}, and the $^7F_1$ level at about 300 cm^{-1}.

The concentration dependence of the vibronic intensity mentioned above, has probably to be explained along the same lines. In view of the interaction range (up to 10 Å) direct 4f–4f interaction seems to be too weak. If, however, higher configurations are mixed in, the range is extended. In fact this concentration dependence is pronounced if another configuration is at relatively low energy (Blasse 1990, Donega and Blasse (1991), see also above). There is not much doubt that also for Eu^{3+}

Table 15. Ratio of the integrated vibronic intensity to the electronic intensity in the $^5D_0$–$^7F_1$ transition of Eu^{3+} in several host lattices, Huang–Rhys factor S, and position of the lowest allowed optical transition in the system (data from Blasse (1990)).

Composition	$\frac{I_{vibr}}{I_{electr}}$	S	Position lowest allowed transition (10^3 cm^{-1})
$SrTiO_3:Eu^{3+}$	3	1·4	25
$Eu_2Mg_3(NO_3)_{12}\cdot 24H_2O$	0·3	0·2	30
$CaWO_4:Eu^{3+}$	0·04	0·04	40

increasing covalency implies increasing vibronic intensity as concluded above for Gd^{3+}.

Recently we have published our first results on the vibronic intensities of Pr^{3+} in several host lattices (Donega and Blasse 1991). It is clear that the vibronic intensities are much stronger for Pr^{3+} than for Gd^{3+} and Eu^{3+}, that the Δ process is much more pronounced, and the concentration dependence seems to be general in the case of Pr^{3+}. These results are confirmed by results by other authors, each on one system (Galczynski and Strek 1991, Yen *et al.* 1964, Hehlen *et al.* 1991, Caro *et al.* 1985).

A possible explanation for stronger vibronic effects in Pr^{3+} in comparison with Gd^{3+} and Eu^{3+} would be the more diffuse character of its 4f wavefunctions due to the lower nuclear charge. In this connection it is interesting to note that also the Nd^{3+} ion seems to show such strong effects (Caro *et al.* 1985), whereas for Yb^{3+} the vibronic lines are weak ($\sim 1\%$) (Dexpert-Ghys and Auzel 1984). It is clear that much research has still to be performed in order to clarify and understand the situation.

3.8. *Relation to other physical phenomena*

In this section we draw attention to some recent publications which are not directed to vibronic transitions in rare earth spectroscopy, but touch on concepts which we have used above.

Powell *et al.* (1990) performed four-wave mixing experiments on Nd^{3+}-doped crystals and glasses. In this way they find that the polarisability of the emitting $^4F_{3/2}$ excited state of Nd^{3+} differs from that of the $^4I_{9/2}$ ground state. This difference, $\Delta\alpha$, varies with the nature of the ligands of the Nd^{3+} ion. In fluorides $\Delta\alpha$ is considerably smaller than in oxides. To cite some values, $\Delta\alpha$ amounts to 0·0107, 0·0464 and 0·096 Å^3 for Nd^{3+} in $Na_2Y_3F_{11}$, $Y_3Al_5O_{12}$ and YVO_4, respectively. In the case of Nd^{3+} ($4f^3$) it is the opposite-parity configuration $4f^25d$ which is mixed into the levels of the $4f^3$ configuration. Obviously the amount of mixing is not equal for the two optical levels involved, nor is it independent of the host lattice. This is exactly the same conclusion which follows from the vibronic spectra discussed above. Powell *et al.* interpret their results using the radial integral $\langle 4f|r|5d\rangle$. Its value appears to depend on the host lattice. In fact this parameter runs parallel with the degree of covalency. It is interesting that so different experiments as four-wave mixing and vibronic spectroscopy lead to the same conclusions, even if they are of a qualitative nature only.

Weaver and Payne (1989) determined polarisability differences of Cr^{3+} in different host lattices. Also here $\Delta\alpha$ varies with the host. For the $^4T_2$ and $^4A_2$ states $\Delta\alpha$ is much larger than for ^2E and $^4A_2$ states. The authors show that $\Delta\alpha$ is larger if the ligand–Cr^{3+} charge-transfer transition is at lower energies. Also here there is a parallel with our conclusions from the vibronic spectra which state that the lower the allowed transitions, the more intense the vibronic lines.

In this connection we mention also work by Williams *et al.* (1989) on Ce^{3+} in a number of different hosts. They derived directly the radial integral $\langle 4f|r|5d\rangle$ which depends on the host. A correlation was found between the value of this integral and the Ce^{3+}–ligand distance which points again to a role of covalency.

Finally we draw attention to the work by Downer's group (Downer *et al.* 1988, Burdick *et al.* 1989). They describe new contributions to the intensity of spin-forbidden electronic transitions of rare earth ions. It cannot be excluded that this is also of importance for the vibronic intensities. The importance of these contributions increases with covalency, so that they will not influence the considerations given above (Sytsma *et al.* 1991).

4. Conclusions and outlook

Vibronic transitions in rare earth spectroscopy have now been observed in many cases, for the intraconfigurational $4f^n$ transitions as well as for the interconfigurational $4f^n$–$4f^{n-1}5d$ transitions. This review discussed mainly the former. We have presented many examples of these transitions, especially in the case of Gd^{3+}. This ion presents in emission a favourable case because of its unsplit ground state ^8S. In this way it was possible to test the present outcome of theoretical approaches. The agreement is satisfying, though not of a quantitative nature.

The intensity of these vibronic transitions is considerably higher than previously expected. This holds for ions like Gd^{3+} and Eu^{3+}, but especially for Pr^{3+} where the vibronic intensity in a given transition can exceed the electronic intensity. It is also clear that contributions from the Δ process (Frank–Condon principle) may be important in certain cases. This implies that the admixture of opposite-parity configurations in the initial and final states may be different for levels within the same $4f^n$ configuration. It is clear that for large effects these admixed configuration should be at low energies. Usually the vibronic intensity becomes concentration dependent in that case.

It seems profitable to us if in the future theoretical calculations would take account of these effects. A nice model system is $SrTiO_3 : Eu^{3+}$ where the effects are very strong. Perhaps there are even more suitable systems which do not need charge compensation in the lattice. For the coming years we expect a better understanding of our knowledge of the way in which the host lattice influences the intensity of these vibronic transitions and of the factors which determine their concentration dependence.

Acknowledgments

The author acknowledges with pleasure an intense cooperation with Dr L. H. Brixner on the vibronic transitions of Gd^{3+} during a couple of years before his retirement from E.I. du Pont de Nemours and Company (Wilmington, USA). He has also profited from the cooperation with Dr A. Meijerink and Dr J. Sytsma in the Utrecht laboratory. Mrs Jessica Heilbrunn carefully typed the manuscript.

References

ANTIC-FIDANCEV, E., LEMAITRE-BLAISE, M., and CARO, P., 1987, *New J. Chem.*, **11**, 467.

AUZEL, F., DE SA', G. F., and DE AZEVEDO, W. M., 1980, *J. Luminescence*, **21**, 187.

BERRY, M. T., KIRBY, A. F., and RICHARDSON, F. S., 1989, *Mol. Phys.*, **66**, 723.

BLASSE, G., 1987 *a*, *Spectroscopy of Solid-State Laser-type Materials*, edited by B. DiBartolo (New York: Plenum), p. 179; 1987 b, *Mater. Chem. Phys.*, **16**, 201;1989, *Chem. Mater.*, **1**, 294; 1990, *Inorg. Chim. Acta*, **167**, 33.

BLASSE, G., BRIL, A., and NIEUWPOORT, W. C., 1966, *J. phys. Chem. Solids*, **27**, 1587.

BLASSE, G., BRIL, A., and SABBATINI, N., 1989, *Chem. Phys. Lett.*, **158**, 504.

BLASSE, G., and BRIXNER, L. H., 1989 *a*, *Eur. J. Solid State Inorg. Chem.*, **26**, 367; 1989 *b*, *Inorg. Chim. Acta*, **161**, 13; 1990 *a*, *Ibid.*, **169**, 25; 1990 *b*, *Recl. Trav. Chim. Pays-Bas.*, **109**, 172.

BLASSE, G., BRIXNER, L. H., and HYATT, G., 1989 *b*, *Chem. Phys. Lett.*, **164**, 617.

BLASSE, G., BRIXNER, L. H., and MROCZKOWSKI, S., 1989 *a*, *J. Solid State Chem.*, **82**, 303.

BLASSE, G., BRIXNER, L. H., and SABBATINI, N., 1989 *d*, *Chem. Phys. Lett.*, **158**, 504.

BLASSE, G., and DIRKSEN, G. J., 1988, *Inorg. Chim. Acta*, **145**, 303; 1992, *J. Solid State Chem.*, **96**, 258.

BLASSE, G., DIRKSEN, G. J., and MEIJERINK, A., 1990, *Chem. Phys. Lett.*, **167**, 41.

BLASSE, G., SYTSMA, J., and BRIXNER, L. H., 1989 *c*, *Chem. Phys. Lett.*, **155**, 64.

BOUAZAOUI, M., JACQUIER, B., LINARES, C., and STREK, W., 1991, *J. Phys. Condens. Matter*, **3**, 921.

BRIXNER, L. H., 1987, *Inorg. Chim. Acta*, **140**, 97.

BRIXNER, L. H., and BLASSE, G., 1989, *Chem. Phys. Lett.*, **157**, 283.

BRIXNER, L. H., CRAWFORD, M. K., and BLASSE, G., 1990, *J. Solid State Chem.*, **85**, 1.

BURDICK, G. W., DOWNER, M. C., and SARDAR, D. K., 1989, *J. Chem. Phys.*, **91,** 1511.
CARO, P., MOUNE, O. K., ANTIC-FIDANCEV, E., and LEMAITRE- BLAISE, M., 1985, *J. less-common metals*, **112,** 153.
DETRIO, J. A., 1971, *Phys. Rev.* B, **4,** 1422.
DEXPERT-GHYS, J., and AUZEL, F., 1984, *J. chem. Phys.*, **80,** 4003.
DIBARTOLO, B., 1968, *Optical Interactions in Solids* (New York: Wiley).
DIRKSEN, G. J., HOFFMAN, A. N. J. M., VAN DE BOUT, T. P., LAUDY, M. P. G., and BLASSE, G., 1991, *J. Mater. Chem.*, **1,** 1001.
DONEGA, C., DE MELLO, and BLASSE, G., 1991, *Chem. Phys. Lett.*, **183,** 367.
DOWNER, M. C., BURDICK, G. W., and SARDAR, D. K., 1988, *J. Chem. Phys.*, **89,** 1787.
FAULKNER, T. R., and RICHARDSON, F. S., 1978, *Molec. Phys.*, **35,** 1141; *Ibid.*, **36,** 193.
FLINT, C. D., 1989, *Vibronic Processes in Inorganic Chemistry* (Dordrecht: Kluwer).
GALCZYNSKI, M., and STREK, W., 1991, *J. Phys. Chem. Solids*, **52,** 681.
HALL, D. W., BRAWER, S. A., and WEBER, M. J., 1982, *Phys. Rev.* B, **25,** 2828.
HAZENKAMP, M. F., and BLASSE, G., 1990, *Chem. Mater.*, **2,** 105.
HAZENKAMP, M. F., VAN DER VEEN, A. M. H., and BLASSE, G., 1992, *J. chem. Soc. Faraday Trans.*, **88,** 133.
HEHLEN, M. P., RIESEN, H., and GÜDEL, H. U., 1991, *Inorg. Chem.*, **30,** 2273.
HENDERSON, B., and IMBUSCH, G. F., 1989, *Optical Spectroscopy of Inorganic Solids* (Oxford: Clarendon Press).
HOSHINA, T., IMANAGA, S., and YOKONO, S., 1977, *J. Luminescence*, **15,** 455.
JUDD, B. R., 1962, *Phys. Rev.*, **127,** 750.
JUDD, 1980, *Physica scripta*, **21,** 543.
KUNDU, L., BANERJEE, A. K., and CHOWDHURY, M., 1991, *Chem. Phys. Lett.*, **181,** 569.
LEVER, A. B. P., 1984, *Inorganic Electronic Spectroscopy*, second edition (Amsterdam: Elsevier).
MEIJERINK, A., NUYTEN, J., and BLASSE, G., 1989, *J. Luminescence*, **44,** 19.
MIYAKAWA, T., 1973, *Luminescence of Crystals, Molecules and Solutions*, edited by F. Williams (New York: Plenum), p. 394.
MORLEY, J. P., FAULKNER, T. R., and RICHARDSON, F. S., 1982, *J. chem. Phys.*, **77,** 1710.
NIEUWPOORT, W. C., BLASSE, G., and BRIL, A., 1967, *Optical Properties of Ions in Crystals*, edited by H. M. Crosswhite and H. W. Moos (New York: Interscience), p. 161.
OFELT, G. S., 1962, *J. chem. Phys.*, **37,** 511.
PEACOCK, R. D., 1975, *Struct. Bonding*, **22,** 83.
POWELL, R. C., PAYNE, S. A., CHASE, L. L., and WILKE, G. D., 1990, *Phys. Rev.* B, **41,** 8593.
REID, M. F., and RICHARDSON, F. S., 1984, *Molec. Phys.*, **51,** 1077.
REISFELD, R., and JØRGENSEN, C. K., 1977, *Lasers and Excited States of Rare Earths* (Berlin: Springer).
RICHARDSON, F. S., REID, M. F., DALLARA, J. J., and SMITH, R. D., 1985, *J. chem. Phys.*, **83,** 3813.
RYAN, F. M., LEHMANN, W., FELDMANN, D. W., and MURPHY, J., 1974, *J. electrochem. Soc.*, **121,** 1475.
STAVOLA, M., ISGANITIS, L., and SCEATS, M. G., 1981 *a*, *J. chem. Phys.*, **74,** 4228.
STAVOLA, M., FRIEDMAN, J. M., STEPNOSKI, R. A., and SCEATS, M. G., 1981 *b*, *Chem. Phys. Lett.*, **80,** 192.
SYTSMA, J., VAN SCHAIK, W., and BLASSE, G., 1991 *a*, *J. Phys. Chem. Solids*, **52,** 419; 1991 *b*, *J. Luminescence*, **48/49,** 494.
SYTSMA, J., and BLASSE, G., 1992, *J. Luminescence*, (in press).
TANNER, P. A., QUAGLIANO, J., and RICHARDSON, F. S., 1991, *J. chem. Soc. Faraday Trans.*, **87,** 1707.
VERWEIJ, J. W. M., IMBUSCH, G. F., and BLASSE, G., 1989, *J. Phys. Chem. Solids*, **50,** 813.
VAN VLIET, J. P. M., BLASSE, G., and BRIXNER, L. H., 1988, *J. Solid State Chem.*, **76,** 160.
VAN VLIET, J. P. M., and BLASSE, G., 1990, *J. Solid State Chem.*, **85,** 56.
DE VRIES, A. J., and BLASSE, G., 1988, *J. Chem. Phys.*, **88,** 7312.
WEAVER, S. C., and PAYNE, S. A., 1989, *Phys. Rev.* B, **40,** 10727.
WILLIAMS, G. M., EDELSTEIN, N., BOATNER, L. A., and ABRAHAM, M. M., 1989, *Phys. Rev.* B, **40,** 4143.
YAMADA, N., and SHIONOYA, S., 1971, *J. phys. Soc. Japan*, **31,** 841.
YAMASHITA, N., YAMAMOTO, I., NINAGAWA, K., WADA, T., YAMASHITA, Y., and NAKAO, Y., 1985, *Japan J. appl. Phys.*, **24,** 1174.
YEN, W. M., SCOTT, W. C., and SCHAWLOW, A. L., 1964, *Phys. Rev.*, **136,** A 271.